Extensive studies on linear growth processes with spatiotemporally correlated noise in arbitrary substrate dimensions

Ning-Ning Pang[*,†]
Department of Physics and Center for Theoretical Sciences, National Taiwan University, Taipei, Taiwan

Wen-Jer Tzeng[*,‡]
Department of Physics, Tamkang University, Tamsui, Taipei, Taiwan

(Received 6 December 2008; revised manuscript received 25 June 2010; published 17 September 2010)

An extensive analytical and numerical study on a class of growth processes with spatiotemporally correlated noise in arbitrary dimension is undertaken. In addition to the conventional investigation on the interface morphology and interfacial widths, we pay special attention to exploring the characteristics of the slope-slope correlation function $S(\mathbf{r},t)$ and the $[Q]$-th degree residual local interfacial width $w[Q](l,t)$, whose importance has been somewhat overlooked in the literature. Based on the above analysis, we give a plausible theoretical explanation about the various experimental observations of kinetically and thermodynamically unstable surface growth. Furthermore, through explicit examples, we show that the statistical methods of calculating the exponents (including the dynamic exponent z, the global roughness exponent α, and the local roughness exponent α_{loc}), based on the scaling of $S(\mathbf{r},t)$ and $w[Q](l,t)$, are very reliable and rarely influenced by the finite time and/or finite-size effects. Another important issue we focus on in this paper is related to numerical calculation. For the specific class of growth processes discussed in this paper, we develop a very efficient and accurate algorithm for numerical calculation of the dynamics of interface configuration, the structure factor, the various correlation functions, the interfacial width and its variants in arbitrary dimensions, even with very large system size and very late time. The proposed systematical algorithm can be easily generalized to other linear processes and some special nonlinear processes.

DOI: 10.1103/PhysRevE.82.031605 PACS number(s): 81.10.Aj, 68.35.Ct, 05.40.−a, 02.50.Ey

I. INTRODUCTION

It has been known for decades that stochasticity plays an important role in various physical processes. If the characteristic spatiotemporal length scales of noise are much smaller than those of the physical system, the employment of white noise is justified. However, in many physical processes, the characteristic length scales of noise and those of the physical system are not well separated, so the stochasticity should be considered as correlated noise. Noises of this type have been widely observed in nature: for instance, the formation of vortices during the transition from normal to superfluid phases of helium-4 and helium-3 [1], the formation of diamond microcrystallites on silicon substrates [2], the appearance of Turing structures in reaction-diffusion systems [3], cross correlation in the activities within neuronal networks [4], and pulse-current electrochemical deposition processes [5]. In addition, various fluctuating systems in Nature consist of global structures, such as amorphous film growth [6,7], physiology signals [8,9], electrochemical deposition [10], and the climatological temperature and salinity distribution of world oceans [11].

In the field of kinetic interfacial roughening, there have been plenty of experimental observations on the *unstable* surface growth phenomena, due to kinetic or thermal instability, for various materials in certain substrate crystalline planes with a wide range of growth temperatures and deposition fluxes. We summarize some important experiments and their observations as follows. These experiments are based on the molecular-beam-epitaxial (MBE) technique, including both heteroepitaxial and homoepitaxial film growth: the growth of Fe (001) films deposited onto Mg (001) substrates, the growth of Ge (001) films on Ge (001) substrates, the growth of Cu (100) crystals, the growth of Fe (001) crystals, and the epitaxially grown GaAs films on GaAs (001) substrates [12–16]. In these experiments, people observe that a pattern of three-dimensional (or two-dimensional) hill-and-valley macroscopic structures evolves with time. As growth time increases, these mounds slowly coalesce and eventually only one on the order of the lateral size of the substrate remains. Quantitatively, the lateral linear size of the mound ξ is observed to increase with time according to a power law $\xi \sim t^{1/z}$ with $z \approx 2,4,6$ depending on the materials, substrate crystalline planes, and the growth temperature. In addition, depending on the materials, the average magnitude of local inclination of the mounds either remains constant in time (the "magic slope") or increases with time following a power law. In view of the arrangement of these macroscopic patterns evolving out of inherent instabilities in growth processes, we believe that it may provide a new route to experimentalists in future technological applications.

However, there still lacks systematical theoretical studies on the interfacial growth equations in arbitrary substrate dimensions with the presence of spatiotemporally correlated noise, which are capable of generating macroscopic structures and thus offer a plausible explanation for various experimental observations. Hence, we are strongly motivated to

*Corresponding author.
†nnp@phys.ntu.edu.tw
‡wjtzeng@mail.tku.edu.tw

take an extensive study on the following class of linear growth equations with spatiotemporally correlated noises in $d+1$ dimensions:

$$\partial_t h(\mathbf{x},t) = (-1)^{m+1}\nu\nabla^{2m}h(\mathbf{x},t) + \eta(\mathbf{x},t) \quad (1)$$

with positive integer m, where $h(\mathbf{x},t)$ denotes the interface height at the comoving frame with the average velocity, $\mathbf{x}$ denotes the position coordinate embedding in the d-dimensional substrate, and $\eta(\mathbf{x},t)$ accounts for all possible sources of kinetic and thermal fluctuations. Here,

$$\overline{\eta(\mathbf{x},t)\eta(\mathbf{x}',t')} = D|\mathbf{x}-\mathbf{x}'|^{2\rho-d}|t-t'|^{2\theta-1} \quad (2)$$

with $0<\rho<1/2$ and $0<\theta<1/2$ to avoid the unphysical divergence and the overbar denoting the average over randomness throughout this paper. Experimentalists have observed that adatom dynamics become more collective, as the growth temperature approaches the melting temperature or the deposition flux increases. Hence, to account for this feature, the noise correlation indices (ρ,θ) contain implicit dependence on the growth temperature and the average magnitude of the deposition flux.

For $m=1$ and 2, the above equation denotes the Edwards-Wilkinson (EW) equation [17] and the Mullins-Wolf-Villain (MWV) equation [18,19], respectively. Especially, the MWV equation has received much attention. Many experiments can be well described by this equation, for instance, growth of Pt sputter deposited on glass at room temperature [7], nickel surfaces grown by pulse-current electrodeposition [10], the brain tumor growth in a petri dish [20], and the growth of amorphous Si films by thermal evaporation with a low substrate temperature [6]. For $m=3$, the first term in the right-hand side of Eq. (1) accounts for the projected "corner" surface free energy if the substrate crystalline plane does not belong to the category of equilibrium crystalline shapes [21,22]. By employing the scaling analysis, one obtains the global roughness exponent $\alpha=m+\rho+2m\theta-d/2$ and the dynamic exponent $z=2m$. Moreover, for this class of growth processes, the presence of noise correlation is always relevant in the renormalization-group (RG) analysis. Namely, it produces a family of continuously changing universality classes. This may provide one of the origins why the value of the roughness exponent reported in various experiments scatters over a considerable range even for the same material with slightly different experimental conditions. Although the experimental realizations for Eq. (1) with $m>3$ have not yet been established, this study is still very important. Since Eq. (1) is exactly solvable, the rigorous extensive study on Eq. (1) can help us to quantitatively understand many facets of kinetic interfacial roughening phenomena. In Ref. [23], we have studied some important statistical quantities of Eq. (1) in $1+1$ dimensions: the equal-time height difference correlation function, the different-time height difference correlation function at the steady state, and the local interfacial orientational instability. In this paper, in addition to investigating the behaviors of the equal-time height difference correlation function in arbitrary substrate dimensions, we would like to undertake an extensive study on two other important statistical quantities: the slope-slope correlation function and the $[Q]$-th degree residual local interfacial width, whose importance has been somewhat overlooked in the literature. The goal of this paper is to rigorously analyze the interplay of the following effects: the substrate dimensionality, surface tension, and the noise correlation, which are three key features determining the transition from stable surface growth to unstable surface growth.

In the study of interface growth, one of the main interests is to classify the growth processes into universality classes. Thus, it is essential that the statistical methods, used in the analysis of experimental data, indeed give reliable estimates of the values of the scaling exponents. The authors of Refs. [24,25], in studying the scaling behavior of the domain size in the XY model and the growth of pyramidlike structures (caused by the Schwoebel effect) on a MBE surface, have proposed a different approach: using the first zero of the slope-slope correlation function, $r_0(t)$, to determine the value of the dynamic exponent z. They surprisingly found that the power-law fit $(t^{1/z})$ to the data was almost perfect for the whole range. Inspired by these numerical works, the author of Ref. [26] chose two phenomenological correlation models, the stretched-exponential correlation model [defined by $\overline{\langle h(\mathbf{x},t)h(\mathbf{x}+\mathbf{r},t)\rangle_L}=\sigma^2 e^{-(r/\xi)^{2\alpha}}$] and the k-correlation model [defined by $\tilde{h}(\mathbf{k},t)\tilde{h}(-\mathbf{k},t)=\frac{\sigma^2\xi^2}{2\pi}(1+ak^2\xi^2)^{-1-\alpha}$], to study the general behavior of the slope-slope correlation function. However, he found that the existence of the first zero and the properties of the slope-slope correlation function strongly depend on the substrate dimensionality and the value of the roughness exponent α. The controversy among Refs. [24–26] motivates us to investigate the following issues. What are the generic properties of the slope-slope correlation function $S(\mathbf{r},t)$ and their dependence on the substrate dimensionality and noise correlation? Is the existence of $r_0(t)$ [the first zero of $S(\mathbf{r},t)$] irrespective of the substrate dimensionality and the values of the scaling exponents? Is the method of determining the dynamic exponent z based on $r_0(t)$ indeed superior to other conventional methods in the literature? In addition to the discussion on the measurement of the dynamic exponent z, we also construct a statistical method (based on the $[Q]$-th degree residual local interfacial width) capable of measuring both the local roughness exponent α_{loc} and the global roughness exponent α.

Another important issue we would like to address in this paper is related to numerical calculation of interfacial growth equations. To obtain the full time evolution of interface dynamics, one usually performs numerical integration by discretizing growth equations on the space-time grid points. The most renowned merit of direct numerical integration is its clarity and simplicity in execution. However, for the growth processes with long relaxation time [such as Eq. (1) with $m\geq 2$], direct numerical integration usually takes tremendous CPU time to obtain the full interfacial dynamics. Therefore, it will be very valuable if one can design an efficient algorithm, without sacrifice of precision, for numerical calculation of growth processes. We are strongly motivated to work out such an algorithm. To demonstrate the excellency of our algorithm, a detailed comparison between our method and the numerical integration strategies given by commercial softwares such as MATHEMATICA will be made.

The outline of this paper is as follows. In Sec. II, we will first analytically work out the exact forms of the interface

height $h(\mathbf{x},t)$, the equal-time height difference correlation function $G(\mathbf{r},t)$, the slope-slope correlation function $S(\mathbf{r},t)$, the local interfacial width $w(l,t)$, and the $[Q]$-th degree residual local interfacial width $w[Q](l,t)$. Then, the implication of the obtained results will be discussed, such as the macroscopic structure formation, anomalous interfacial roughening, and the role of noise, etc. Subsequently, special attention will be paid to exploring the characteristics of $S(\mathbf{r},t)$ and $w[Q](l,t)$. We will investigate in detail the statistical methods of measuring the exponents, based on the scaling of $w[Q](l,t)$ and the first zero of $S(\mathbf{r},t)$. In Sec. III, we will first discuss the general method of numerical calculation of interface growth equations. The explicit and general expressions of $G(\mathbf{r},t)$, $S(\mathbf{r},t)$, $w(l,t)$, and $w[Q](l,t)$ via the structure factors will be obtained. Then, for the class of growth processes discussed in this paper, we will employ the above expressions and construct a very efficient and accurate algorithm for numerical calculation of these statistical quantities in arbitrary dimensions, even with very large system size and very late time. In Sec. IV, a brief summary will be given.

II. INTERFACE DYNAMICS

For the purpose of self-containedness, we first briefly review the basic concepts in the context of interfacial roughening [27]. It is widely observed that global interfacial widths $w(L,t)$ obey the ordinary dynamic scaling ansatz,

$$w(L,t) \sim \begin{cases} t^{\alpha/z}, & \text{for } t \ll L^z, \\ L^{\alpha}, & \text{for } t \gg L^z, \end{cases} \tag{3}$$

with L denoting the linear side length of the d-dimensional substrate. The exponents α and z are known as the global roughness exponent and the dynamic exponent, respectively. People have also both experimentally [6,7,10] and theoretically [28,29] observed that the equal-time height difference correlation function $G(\mathbf{r},t)$ and the local interfacial width $w(l,t)$ obey the following generalized dynamic scaling ansatz,

$$G(\mathbf{r},t) \sim \begin{cases} t^{2\alpha/z}, & \text{for } t \ll r^z, \\ r^{2\alpha_{\mathrm{loc}}} t^{2(\alpha-\alpha_{\mathrm{loc}})/z}, & \text{for } r^z \ll t \ll L^z, \\ r^{2\alpha_{\mathrm{loc}}} L^{2(\alpha-\alpha_{\mathrm{loc}})}, & \text{for } t \gg L^z, \end{cases} \tag{4}$$

and

$$w^2(l,t) \sim \begin{cases} t^{2\alpha/z}, & \text{for } t \ll l^z, \\ l^{2\alpha_{\mathrm{loc}}} t^{2(\alpha-\alpha_{\mathrm{loc}})/z}, & \text{for } l^z \ll t \ll L^z, \\ l^{2\alpha_{\mathrm{loc}}} L^{2(\alpha-\alpha_{\mathrm{loc}})}, & \text{for } t \gg L^z, \end{cases} \tag{5}$$

with $\mathbf{r}$ and l denoting the displacement vector in the d-dimensional substrate space and the side length of a d-dimensional local observation window, respectively. For the systems displaying ordinary dynamic scaling behaviors, one has the value of the local roughness exponent α_{loc} equal to that of the global roughness exponent α. In contrast, for the systems displaying anomalous dynamic scaling behaviors, these two exponents are independent.

Subsequently, let us turn to the analysis of the interface growth equation Eq. (1). The flat initial condition and the periodic boundary condition are imposed. The Fourier transformation of Eq. (1) into $\mathbf{k}$-space is given as

$$\partial_t \tilde{h}(\mathbf{k}_{\mathbf{n}},t) = -\nu k_{\mathbf{n}}^{2m} \tilde{h}(\mathbf{k}_{\mathbf{n}},t) + \tilde{\eta}(\mathbf{k}_{\mathbf{n}},t), \tag{6}$$

with $\mathbf{k}_{\mathbf{n}} \equiv (\frac{2\pi n_1}{L}, \ldots, \frac{2\pi n_d}{L})$ and $n_i = 0, \pm 1, \pm 2, \ldots$. The corresponding noise correlation in $\mathbf{k}$-space is then derived as

$$\overline{\tilde{\eta}(\mathbf{k}_{\mathbf{n}},t)\,\tilde{\eta}(\mathbf{k}_{\mathbf{n}'},t')} = D_\rho k_{\mathbf{n}}^{-2\rho} |t-t'|^{2\theta-1} \left[\prod_{i=1}^{d} L \delta_{n_i,-n_i'} \right], \tag{7}$$

with $D_\rho = D \cdot \frac{2\pi^{(d-1)/2}\Gamma(2\rho)\cos(\rho\pi)\Gamma(1/2-\rho)}{\Gamma(d/2-\rho)}$ and $\Gamma(x)$ denoting the Gamma function. Note that, for the continuum system, the noise correlation index $\rho=0$ ($\theta=0$) will give rise to the ultraviolet divergence of noise correlation in $\mathbf{k}$-space (ω-space). This phenomenon has been observed in the Kardar-Parisi-Zhang (KPZ) equation with spatiotemporally correlated noises [30,31]. In the literature, people usually introduce an upper cutoff in $\mathbf{k}$-space (ω-space) to rescue the divergence problem. Although the upper cutoff in $\mathbf{k}$-space can be regarded as the reciprocal of the lattice constant in real physical systems, no physical arguments have been proposed to explain the upper cutoff in ω-space. Hence, we do not include the cases with the noise correlation indices $\rho=0$ or $\theta=0$ for clarity of this paper. The solution of Eq. (1) is obtained as

$$\begin{aligned} h(\mathbf{x},t) &= \frac{1}{L^d} \sum_{\mathbf{n}} e^{i\mathbf{k}_{\mathbf{n}}\cdot\mathbf{x}} \int_0^t d\tau \tilde{\eta}(\mathbf{k}_{\mathbf{n}},\tau) e^{-\nu k_{\mathbf{n}}^{2m}(t-\tau)} \\ &= \frac{1}{L^d} \sum_{\mathbf{n}} \int_0^t d\tau \int \cdots \int_{L^d} d^d\mathbf{r}\, \eta(\mathbf{x}+\mathbf{r},\tau) e^{-i\mathbf{k}_{\mathbf{n}}\cdot\mathbf{r} - \nu k_{\mathbf{n}}^{2m}(t-\tau)}. \end{aligned} \tag{8}$$

We then develop a very efficient numerical scheme to simulate the interface configuration of these growth processes, even with very large lateral system size and growth time for arbitrary substrate dimension. The details of the numerical algorithm will be given in the next section.

The growth equation Eq. (1) displays very rich interfacial features, including smooth interfacial growth (the exponent $\alpha=0$), normal roughening growth ($\alpha<1$), and unstable surface growth ($\alpha>1$). The substrate dimension d_{uc} is defined as the upper critical substrate dimension, above which the interface growth is in the smooth regime. The substrate dimension d_{lc} is defined as the lower critical substrate dimension, below which the interface growth is in the regime of unstable surface growth. With fixed values of (m,ρ,θ), the dimensions d_{uc} and d_{lc} are equal to $2m+[2\rho+4m\theta]$ and $2m-1+[2\rho+4m\theta]$, respectively, with $[\cdot]$ denoting the integer part of the argument throughout this paper. In this paper, we focus on the interfacial roughening phenomena, i.e., the global roughness exponent $\alpha = m+\rho+2m\theta-d/2 > 0$. One of the most distinct features of the growth equation Eq. (1) is that it consists of continuously changing universality classes, if a universality class is classified by the scaling exponents. Specifically, the global roughness exponent α $[=m+\rho+2m\theta-d/2]$ is a strictly increasing function of the noise correlation indices (ρ,θ) for the whole range. This property is very different from the KPZ growth processes with spatiotempo-

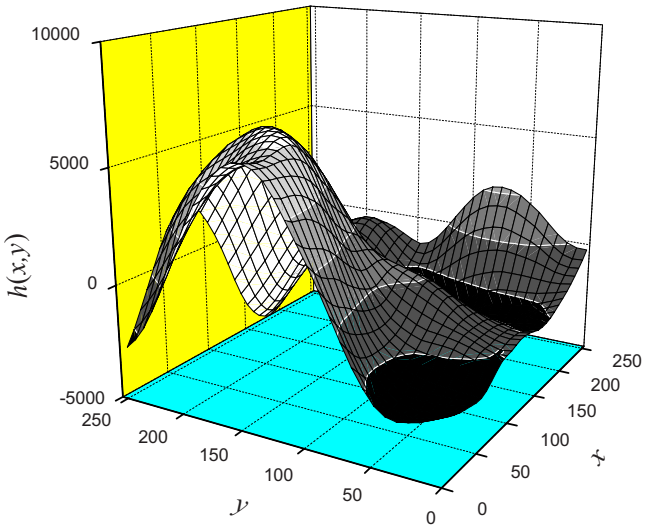

FIG. 1. (Color online) A typical interface morphology for the growth processes governed by Eq. (1) with the global roughness exponent $\alpha > 1$. The data are generated with the parameter $m=2$, the substrate dimension $d=2$, the noise correlation indices $(\rho, \theta) = (0.3, 0.3)$, and, accordingly, the exponent $\alpha = 2.5$.

rally correlated noises [30,31]. For the KPZ cases, there exists a stability boundary (ρ_c, θ_c) separating the dominant region of the white-noise fixed point from that of the long-range noise fixed point: The global roughness exponent α is a strictly increasing function of (ρ, θ) only above this boundary, while the exponent α always equals α (white noise) below this boundary.

Figure 1 shows a snapshot of typical interface morphology within a local observation window for the growth process with the exponent $\alpha > 1$. Pictorially, the interfaces gradually develop large hill-and-valley structures as the growth time increases. More specifically, small mounds are coalescing to form large mounds and the average magnitude of local inclination of the mounds also increases with time. Eventually, the effect of finite lateral system size enters and restricts further development of large mounds. At late times, the lateral linear characteristic length scale ξ of the remaining large mounds is in the order of lateral linear system size L. The above observed distinct feature can be understood as follows. In principle, the stochastic fluctuation of the deposition flux and the adatom nucleation process induce the roughness, which is counterbalanced by a smoothing effect due to surface tension. However, if the surface growth is unstable, the competition between roughening and smoothing can reach an equilibrium only on a short spatial range, but macroscopically the roughness continues to evolve and results in a hill-and-valley pattern formation. Note that making use of these macroscopic patterns out of inherent instability in surface growth may provide a new path for further technological applications.

For unstable surface growth evolving out of a flat substrate, its signature characteristic is that the relative global saturated surface width $w_{\mathrm{sat}}(L)/L$ does not vanish in the thermodynamic limit (i.e., $L \to \infty$) and this sets the lower limit of the corresponding global roughness exponent α being one. The three microscopic atomistic mechanisms causing unstable surface growth are long-range correlation of adatom dynamics, thermal faceting, and Schwoebel barriers. In the following, we will briefly discuss these three mechanisms and their generic features. First, let us look at the correlated adatom dynamics. Commonly observed in experiments, adatom dynamics becomes more collective as the deposition flux increases or the growth temperature approaches the melting temperature. The correlation in the nucleation process is attributed to the collective effect of long-range electric-dipole interactions. As a result, surface fluctuations also become long-range positively correlated and are capable of forming macroscopic hill-and-valley patterns. The second mechanism causing unstable surface growth is thermal faceting. At a fixed growth temperature, the category of equilibrium crystal shape (ECS) can be obtained through Wulff construction in terms of the Legendre transform of the surface free energy [21,22]. If the initial substrate crystalline plane belongs to the category of ECS, one expects a stable surface growth with moderate degree of roughness due to thermal fluctuation. However, if the initial substrate crystalline plane does not lie inside this category, surface instability results in thermal faceting. Accordingly, the average magnitude of local interface inclination will gradually develop as growth time increases. In general, with lower growth temperature, the range of ECS will narrow down and the sharpness of faceted growth will increase. The third mechanism inducing unstable surface growth is the presence of strong Schwoebel barriers. At low growth temperature, the diffusion bias of adatoms due to step edge barriers (Schwoebel barriers) is significant, which results in a net uphill surface current. Namely, adatoms preferably attach to steps from the terrace below rather than from above. Consequently, small islands nucleate on top of preexisting islands and gradually develop large mounds. If the origin of unstable surface growth is purely due to step edge barriers (Schwoebel barriers), one expects a regular pattern of pyramid-like growth mounds and their slopes are characterized by a constant "magic slope." Hence, the corresponding global roughness exponent α should be equal to one.

Note that, without deliberate control of experimental conditions, the above three mechanisms are interwoven and all contribute to the formation of macroscopic structures. Therefore, the aim of Eq. (1) is to give a generic phenomenological continuum description of both stable surface growth and unstable surface growth, without referring to atomistic details. The first term in the right-hand side of Eq. (1) represents the smoothing effect. Since both effects of step edge barriers and thermal faceting become more significant with decreasing temperature, we set the integer m being an implicit decreasing step function of the growth temperature to account for this tendency. The second term in the right-hand side of Eq. (1) represents the long-range noise correlation. To be consistent with experimental observations, we set the noise correlation indices (ρ, θ) being implicit increasing functions of the deposition flux and the growth temperature. Interestingly, the growth temperature actually plays a double-edged knife in surface roughening. More specifically, with increasing temperature, the values of (ρ, θ) become larger but the value of m either becomes smaller or remains the same. Accordingly, as the growth temperature increases, the

surface may become either rougher or smoother, which depends on the materials and the initial experimental conditions. This accounts for the fact that the experimental reports in the literature, regarding the temperature influence on surface roughening, are so diverse [12–16].

Subsequently, in order to obtain a deeper understanding on this class of growth processes, we will take an extensive study on four important statistical quantities: the equal-time height difference correlation function, the slope-slope correlation function, the local interfacial width, and the $[Q]$-th degree residual local interfacial width.

A. Equal-time height difference correlation function

In this subsection, an extensive analysis of the equal-time height difference correlation function $G(\mathbf{r},t)$ will be undertaken. We will rigorously derive the asymptotes of $G(\mathbf{r},t)$ in successive time regimes and discuss the implications. $G(\mathbf{r},t)$ is defined as

$$G(\mathbf{r},t) \equiv \overline{\langle [h(\mathbf{x},t) - h(\mathbf{x}+\mathbf{r},t)]^2 \rangle_L}, \tag{9}$$

where $\langle \cdots \rangle_L$ denotes the spatial average over the d-dimensional substrate with lateral linear size L throughout this paper. In Ref. [23], we have used a straightforward method to derive the asymptotes of $G(r,t)$ in $1+1$-dimensions. Although the concepts of that method [23] are very simple, it cannot be applied to derive the asymptotes of $G(\mathbf{r},t)$ in higher dimensions. Since $G(\mathbf{r},t)$ is a very fundamental statistical quantity, from which the asymptotes of the slope-slope correlation function, the local interfacial width, and the residual local interfacial width can be further derived, we design a different calculation scheme, capable of obtaining the asymptotes of $G(\mathbf{r},t)$ in arbitrary dimensions. In the following, we will explain in detail the new calculation scheme and explicitly compare these two methods.

By substituting Eqs. (7) and (8) into the above definition of $G(\mathbf{r},t)$ and with some simple calculation, one gets

$$G(\mathbf{r},t) = \frac{2D_\rho}{L^d \nu} \sum_{\mathbf{n}\neq\mathbf{0}} \frac{1-\cos(\mathbf{k_n}\cdot\mathbf{r})}{k_{\mathbf{n}}^{2m+2\rho}} \times \int_0^t d\tau (e^{-\nu k_{\mathbf{n}}^{2m}\tau} - e^{-\nu k_{\mathbf{n}}^{2m}(2t-\tau)}) \tau^{2\theta-1}. \tag{10}$$

For large lateral linear size L, the above summation over $\mathbf{n}$ can be approximated by integration over the whole d-dimensional $\mathbf{k}$-space with an isotropic hole of unit volume centered at the origin. Namely,

$$G(\mathbf{r},t) \simeq \frac{4D_\rho}{(2\pi)^d \nu^{1+2\theta}} \int_{k_0}^{\infty} k^{d-1-2m-2\rho-4m\theta} dk \times \int_0^{\nu k^{2m} t} d\tau (e^{-\tau} - e^{-(2\nu k^{2m} t - \tau)}) \tau^{2\theta-1} \times \left\{ \delta_{d,1}[1-\cos(kr)] + (1-\delta_{d,1}) \times \left(\prod_{j=1}^{d-1} \int_0^{\pi} \sin^{d-1-j}\theta_j d\theta_j \right) [1-\cos(kr\cos\theta_1)] \right\} \tag{11}$$

with δ denoting the Kronecker delta and $k_0 \equiv 2\sqrt{\pi}[\Gamma(d/2+1)]^{1/d}/L$. With a close look at Eq. (11), we observe that there exists a characteristic wave-vector k_c $(\equiv (\nu t)^{-1/(2m)})$ and the temporal evolution of $G(\mathbf{r},t)$ can be categorized into three regimes: $k_c \gg 1/r$, $1/r \gg k_c \gg 1/L$, and $k_c \ll 1/L$. In the following, we will derive the early, intermediate, and late-time asymptotes of $G(\mathbf{r},t)$ from Eq. (11).

1. Early-time asymptote

For the early time regime $(k_c \gg 1/r \gg 1/L)$, we have

$$G(\mathbf{r},t)|_{k_c \gg 1/r} \approx \frac{4D_\rho k_c^{d-2m-2\rho-4m\theta}}{(2\pi)^d \nu^{1+2\theta}} \int_0^{\infty} \xi^{d-1-2m-2\rho-4m\theta} d\xi \times \int_0^{\xi^{2m}} d\tau (e^{-\tau} - e^{-(2\xi^{2m}-\tau)}) \tau^{2\theta-1} \times \left\{ \delta_{d,1}[1-\cos(k_c r\xi)] + (1-\delta_{d,1}) \times \left(\prod_{j=1}^{d-1} \int_0^{\pi} \sin^{d-1-j}\theta_j d\theta_j \right) \times [1-\cos(k_c r\xi\cos\theta_1)] \right\}. \tag{12}$$

In the early time regime, $k_c r$ is large and the cosine term oscillates so quickly that the corresponding term almost cancels in the integration over the ξ-space. Hence, the above integration can be approximated as a constant and we then get

$$G(\mathbf{r},t)|_{k_c \gg 1/r} \sim O\left(\frac{D_\rho}{\nu^{1+2\theta}} k_c^{d-2m-2\rho-4m\theta} \right). \tag{13}$$

Recall that the global roughness exponent $\alpha = m+\rho+2m\theta - d/2$, the dynamic exponent $z=2m$, and the characteristic wave-vector $k_c \equiv (\nu t)^{-1/(2m)}$. The early time asymptote of $G(\mathbf{r},t)$ can be recast as

$$G(\mathbf{r},t)|_{\nu t \ll r^z} \sim O\left(\frac{D_\rho}{\nu^{(d-2\rho)/z}} t^{2\alpha/z} \right). \tag{14}$$

2. Intermediate-time asymptote

For the intermediate time regime $(1/r \gg k_c \gg 1/L)$, we first employ the relations: $J_{-1/2}(y) = \sqrt{\frac{2}{\pi y}}\cos y$ and $\int_0^{\pi} \cos(y\cos x)\sin^{2\mu} x dx = \sqrt{\pi}(2/y)^{\mu}\Gamma(\mu+1/2)J_{\mu}(y)$, and rewrite Eq. (11) as

$$G(\mathbf{r},t)|_{1/r\gg k_c\gg 1/L} \approx \frac{D'_\rho}{\Gamma(d/2)} k_c^{d-2m-2\rho-4m\theta} \int_0^\infty d\tau \tau^{2\theta-1} \times \int_{\tau^{1/(2m)}}^\infty d\xi \xi^{d-2m-2\rho-4m\theta-1} \times (e^{-\tau} - e^{-(2\xi^{2m}-\tau)}) \left[1 - \Gamma\left(\frac{d}{2}\right) \times \left(\frac{2}{k_c r\xi}\right)^{d/2-1} J_{d/2-1}(k_c r\xi) \right] \quad (15)$$

with $D'_\rho \equiv 2^{2-d} D_\rho / (\pi^{d/2} \nu^{1+2\theta})$ and $J_\mu(y)$ denoting the Bessel function of the first kind [32].

Let us first briefly review the method we used in Ref. [23] and explain the reasons why it cannot be generalized to arbitrary dimensions. (a) To simplify the calculation of the double integrals in Eq. (12) of Ref. [23], we changed the integration order and performed the integration over τ first by separating the factor $(e^{-\tau}-e^{-2x^{2m}+\tau})$ into two and employing the two relations below Eq. (14) of Ref. [23]. (b) However, since the term $f(x)$ inside the integrand contains a factor $x^{-2m-2\rho-4m\theta}$, this separation of the terms may cause the integration over x blowing up at $x=0$ for certain terms. (This does not mean that the double integral diverges. It is simply due to the separation of terms.) Hence, we decided to conduct integration by parts over x systematically to raise the exponent in the factor $x^{-2m-2\rho-4m\theta}$ to avoid the incurrence of the divergence at $x=0$, by noting that

$$\int_0^\infty d\tau \tau^{2\theta-1} \int_{\tau^{1/(2m)}}^\infty dx x^{-2\rho-4m\theta+n} g(x,\tau) = \int_0^\infty dx x^{-2\rho-4m\theta+n} \int_0^{x^{2m}} d\tau \tau^{2\theta-1} g(x,\tau) = \int_0^\infty dx x^{-2\rho+n} \int_0^1 dy y^{2\theta-1} g(x,x^{2m}y)$$

is integrable for all $n \geq 0$ with the function $g(x,x^{2m}y)$ being finite at $x=0$. We thus derived Eq. (15) of Ref. [23]. This step is the key point for deriving the intermediate time asymptote of $G(r,t)$ in Ref. [23]. (c) Finally, by conducting the power series expansion for both $\sin(\cdot)$ and $\cos(\cdot)$ in Eq. (15) of Ref. [23] (except the last term) and employing the relations below Eq. (15) of Ref. [23], we then derived Eqs. (16)–(19) of Ref. [23] [the one-dimensional intermediate time asymptote of $G(r,t)$]. (d) In addition, the mathematical formula above Eq. (16) of Ref. [23] (taken from Ref. [32]) actually fails when $2\rho+4m\theta$ being an odd positive integer, the results following this mathematical formula in Ref. [23] only work for the cases with the global roughness exponent being a noninteger. (e) In comparison, Eq. (15) in this paper plays a similar role as Eq. (12) of Ref. [23]. If we still use the calculation scheme of [23] by changing the integration order from $\int_0^\infty d\tau \int_{\tau^{1/(2m)}}^\infty d\xi$ to $\int_0^\infty d\xi \int_0^{\xi^{2m}} d\tau$ and splitting the factor $(e^{-\tau}-e^{-2\xi^{2m}+\tau})$ into two, we will again face the divergent problem for each term at $\xi=0$. Recall that the goal for performing systematic integration by parts over ξ is to raise the exponent in $\xi^{d-2m-2\rho-4m\theta-1}$ and keep other factors being finite at $\xi=0$. However, the procedure of integration by parts cannot always fulfill this goal for arbitrary value of d (dimensionality). Hence, we must take other schemes for computing the double integral of Eq. (15).

In the following, we will separately discuss the cases with the exponent α being a noninteger or an integer.

(i) For the cases with the exponent α being a noninteger: We first need to compute the following integral:

$$\begin{aligned} &\int_{\tau^{1/(2m)}}^\infty d\xi \xi^{d-2m-2\rho-4m\theta-1} (e^{-\tau} - e^{-(2\xi^{2m}-\tau)}) \times \left[1 - \Gamma\left(\frac{d}{2}\right) \left(\frac{2}{k_c r\xi}\right)^{d/2-1} J_{d/2-1}(k_c r\xi) \right] \\ &= -e^{\tau} \int_{\tau^{1/(2m)}}^\infty d\xi \xi^{d-2m-2\rho-4m\theta-1} e^{-2\xi^{2m}} \times \left[1 - \Gamma\left(\frac{d}{2}\right) \left(\frac{2}{k_c r\xi}\right)^{d/2-1} J_{d/2-1}(k_c r\xi) \right] \\ &\quad + e^{-\tau} \int_{\tau^{1/(2m)}}^\infty d\xi \xi^{d-2m-2\rho-4m\theta-1} \times \left[1 - \Gamma\left(\frac{d}{2}\right) \left(\frac{2}{k_c r\xi}\right)^{d/2-1} J_{d/2-1}(k_c r\xi) \right] \equiv I_1 + I_2. \end{aligned} \quad (16)$$

By employing the power series expansion of $J_\mu(y)$ $[=\Sigma_{l=0}^\infty \frac{(-1)^l}{l!\Gamma(\mu+l+1)} (\frac{y}{2})^{2l+\mu}]$ and the mathematical relation

$$\int_y^\infty y^\lambda e^{-2y^{2m}} dy = \frac{2^{-(\lambda+1)/(2m)}}{2m} \Gamma\left(\frac{\lambda+1}{2m}, 2y^{2m}\right) \quad (17)$$

with $\Gamma(a,b)$ denoting the incomplete Gamma function [32], the integral I_1 is obtained as

$$I_1 = \frac{e^\tau \Gamma(d/2)}{2m} \sum_{l=1}^\infty \frac{(-1)^l 2^{-(2l+d-2m-2\rho-4m\theta)/(2m)}}{l!\Gamma(d/2+l)} \times \Gamma\left(\frac{2l+d-2m-2\rho-4m\theta}{2m}, 2\tau\right) \left(\frac{k_c r}{2}\right)^{2l}. \quad (18)$$

By employing the mathematical formula [32]

$$\int_y^\infty y^\lambda J_\mu(y) dy = \frac{2^\lambda \Gamma\left(\frac{\mu+\lambda+1}{2}\right)}{\Gamma\left(\frac{\mu-\lambda+1}{2}\right)} - \sum_{l=0}^\infty \frac{(-1)^l y^{\mu+\lambda+2l+1}}{2^{\mu+2l}(\mu+\lambda+2l+1)\Gamma(\mu+l+1)l!} \quad (19)$$

with $[\mathrm{Re}(\lambda) < 1/2]$, the integral I_2 is obtained as

$$I_2 = e^{-\tau}\Gamma\left(\frac{d}{2}\right) \times\left[\sum_{l=1}^{\infty}\frac{(-1)^l\tau^{(2l+d-2m-2\rho-4m\theta)/(2m)}}{l!(2l+d-2m-2\rho-4m\theta)\Gamma(l+d/2)}\left(\frac{k_c r}{2}\right)^{2l} - \frac{\Gamma(d/2-m-\rho-2m\theta)}{2\Gamma(m+\rho+2m\theta)}\left(\frac{k_c r}{2}\right)^{2m+2\rho+4m\theta-d}\right]. \quad (20)$$

By employing the mathematical relation $[\mu\Gamma(\mu,y)+y^{\mu}e^{-y}=\Gamma(\mu+1,y)$ with $\mu\neq 0]$ to combine Eqs. (18) and (20), we derive

$$G(\mathbf{r},t)|_{1/r\gg k_c\gg 1/L} \approx D'_{\rho}k_c^{d-2m-2\rho-4m\theta}\int_0^{\infty}d\tau\tau^{2\theta-1} \times\left[-e^{-\tau}\frac{\Gamma\left(\frac{d}{2}-m-\rho-2m\theta\right)}{2\Gamma(m+\rho+2m\theta)}\left(\frac{k_c r}{2}\right)^{2m+2\rho+4m\theta-d} + e^{\tau}\sum_{l=1}^{\infty}\frac{(-1)^l 2^{-(2l+d-2m-2\rho-4m\theta)/(2m)}}{l!(2l+d-2m-2\rho-4m\theta)\Gamma\left(\frac{d}{2}+l\right)} \times\Gamma\left(\frac{2l+d-2\rho-4m\theta}{2m},2\tau\right)\left(\frac{k_c r}{2}\right)^{2l}\right]. \quad (21)$$

Then, after some tedious calculation and using the relation

$$\int_0^{\infty}y^{\mu-1}e^{cy}\Gamma(a,by)dy = b^{-\mu}\Gamma(\mu+a)\int_0^{\infty}e^{-\mu t}\left(1-\frac{c}{b}e^{-t}\right)^{-\mu-a}dt = \Gamma(\mu+a)c^{-\mu}B\left(\mu,-\mu-a+1;\frac{c}{b}\right) \quad (22)$$

with $[\mathrm{Re}(b+c)>0,\ \mathrm{Re}\ \mu>0,\ \mathrm{Re}(\mu+a)>0]$ and $B(a,b;y)$ denoting the incomplete Beta function [32], we eventually obtain the intermediate time asymptote of $G(\mathbf{r},t)$ as

$$G(\mathbf{r},t)|_{1/r\gg k_c\gg 1/L} \approx Ar^{2m+2\rho+4m\theta-d}+\sum_{l=1}^{\infty}A_l k_c^{d-2m-2\rho-4m\theta}(k_c r)^{2l} \quad (23)$$

with the coefficients

$$A = -\frac{D'_{\rho}\Gamma(2\theta)\Gamma(d/2-m-\rho-2m\theta)}{2^{2m+2\rho+4m\theta-d+1}\Gamma(m+\rho+2m\theta)} \quad (24)$$

and

$$A_l = \frac{(-1)^l D'_{\rho}2^{1+2\theta-2l+(2\rho-d-2l)/(2m)}}{(2l+d-2m-2\rho-4m\theta)\Gamma\left(\frac{d}{2}+l\right)l!} \times\Gamma\left(\frac{2l+d-2\rho}{2m}\right)B\left(2\theta,\frac{2m+2\rho-d-2l}{2m};\frac{1}{2}\right). \quad (25)$$

This result is generally applicable for arbitrary substrate dimension d. The coefficients in Eqs. (17) and (18) of Ref. [23] can be recast in the same form as Eqs. (24) and (25) in this paper, by employing the following relations and with some calculation:

$$\Gamma(2x)=\frac{2^{2x-1}}{\sqrt{\pi}}\Gamma(x)\Gamma\left(x+\frac{1}{2}\right),$$

$$\Gamma(1-x)\Gamma(x)=\pi\csc(\pi x),$$

$$\Gamma\left(\frac{1}{2}-x\right)\left(\frac{1}{2}+x\right)=\pi\sec(\pi x),$$

$$(x+y)B\left(y,1+x;\frac{1}{2}\right)=2^{-x-y}+xB\left(y,x;\frac{1}{2}\right). \quad (26)$$

By substituting the dynamic exponent $z=2m$, and the characteristic wave-vector $k_c=(\nu t)^{-1/(2m)}$ into Eq. (23), the intermediate time asymptote of $G(\mathbf{r},t)$ can then be recast as

$$G(\mathbf{r},t)|_{L^z\gg\nu t\gg r^z}\approx Ar^{2\alpha}+\sum_{l=1}^{\infty}A_l(\nu t)^{2(\alpha-l)/z}r^{2l}. \quad (27)$$

For the system with the global roughness exponent $\alpha<1$, the leading term in Eq. (27) is $r^{2\alpha}$. Hence, the system displays ordinary dynamic scaling behaviors. In contrast, for the system with the global roughness exponent $\alpha>1$, the terms $((\nu t)^{2(\alpha-1)/z}r^2,\cdots,(\nu t)^{2(\alpha-[\alpha])/z}r^{2[\alpha]})$ are all dominant over the term $r^{2\alpha}$ in Eq. (27), with $[\alpha]$ denoting the integer part of α throughout this paper.

(ii) For the cases with the exponent α being an integer:

The integral I_1 is still given by Eq. (18). Beyond our original expectation, it turns out that the computation of the integral I_2 is extremely complicated. Note that the mathematical formula Eq. (19) (given by Ref. [32]) actually fails if $\mu+\lambda$ is an odd negative integer. This is exactly the situation we encounter here. However, we have checked through many mathematical handbooks and no corresponding mathematical formula is found. In the Appendix, we give a rigorous derivation of the integral $\int_x^{\infty}dx x^{-2\alpha-d/2}J_{d/2-1}(x)$ with $\alpha(=m+\rho+2m\theta-d/2)$ being an integer. By using Eq. (A1) derived in the Appendix, we have

$$I_2 = e^{-\tau}\Gamma\left(\frac{d}{2}\right)\left\{\sum_{l=1,l\neq\alpha}^{\infty}\frac{(-1)^l\tau^{(2l+d-2m-2\rho-4m\theta)/(2m)}}{l!(2l+d-2m-2\rho-4m\theta)\Gamma\left(\frac{d}{2}+l\right)}\left(\frac{k_c r}{2}\right)^{2l}\right.$$
$$\left.+\frac{(-1)^{1+m+\rho+2m\theta-d/2}}{\Gamma\left(m+\rho+2m\theta-\frac{d}{2}+1\right)\Gamma(m+\rho+2m\theta)}\left(\frac{k_c r}{2}\right)^{2m-d+2\rho+4m\theta}[\Omega-\ln(k_c r\tau^{\frac{1}{2m}})]\right\} \quad (28)$$

with the value of the coefficient Ω given in Eq. (A2) of the Appendix. Subsequently, by employing the relation $\Gamma(\mu+1,y)=\mu\Gamma(\mu,y)+y^{\mu}e^{-y}$ with $\mu\neq 0$ to combine I_1 [Eq. (18)] and I_2 [Eq. (28)], we obtain

$$\int_{\tau^{1/2m}}^{\infty} d\xi\xi^{d-2m-2\rho-4m\theta-1}(e^{-\tau}-e^{-(2\xi^{2m}-\tau)})\left[1-\Gamma\left(\frac{d}{2}\right)\left(\frac{2}{k_c r\xi}\right)^{d/2-1}J_{d/2-1}(k_c r\xi)\right]$$
$$=\Gamma\left(\frac{d}{2}\right)\left\{\frac{(-1)^{1+m+\rho+2m\theta-d/2}}{\Gamma\left(m+\rho+2m\theta-\frac{d}{2}+1\right)\Gamma(m+\rho+2m\theta)}\left(\frac{k_c r}{2}\right)^{2m+2\rho+4m\theta-d}\times\left[e^{-\tau}\left(\Omega-\ln(k_c r)-\frac{1}{2m}\ln\tau\right)-\frac{e^{\tau}}{2m}\Gamma(0,2\tau)\right]\right.$$
$$\left.+e^{\tau}\sum_{l=1,l\neq\alpha}^{\infty}\frac{(-1)^l 2^{1+2\theta-(2l+d-2\rho)/(2m)}}{l!(2l+d-2m-2\rho-4m\theta)\Gamma\left(\frac{d}{2}+l\right)}\Gamma\left(\frac{2l+d-2\rho}{2m}-2\theta,2\tau\right)\left(\frac{k_c r}{2}\right)^{2l}\right\}. \quad (29)$$

Hence, we get

$$G(\mathbf{r},t)|_{1/r\gg k_c\gg 1/L}\approx D'_{\rho}k_c^{d-2m-2\rho-4m\theta}\int_0^{\infty}d\tau\tau^{2\theta-1}\left\{\frac{(-1)^{1+m+\rho+2m\theta-d/2}}{\Gamma\left(m+\rho+2m\theta-\frac{d}{2}+1\right)\Gamma(m+\rho+2m\theta)}\right.$$
$$\times\left(\frac{k_c r}{2}\right)^{2m+2\rho+4m\theta-d}\left[e^{-\tau}\left(\Omega-\ln(k_c r)-\frac{1}{2m}\ln\tau\right)-\frac{e^{\tau}}{2m}\Gamma(0,2\tau)\right]$$
$$\left.+e^{\tau}\sum_{l=1,l\neq\alpha}^{\infty}\frac{(-1)^l 2^{1+2\theta-(2l+d-2\rho)/(2m)}}{l!(2l+d-2m-2\rho-4m\theta)\Gamma\left(\frac{d}{2}+l\right)}\Gamma\left(\frac{2l+d-2\rho}{2m}-2\theta,2\tau\right)\left(\frac{k_c r}{2}\right)^{2l}\right\}. \quad (30)$$

By employing the relations: Eq. (22), $B(\mu,1-\mu;\frac{1}{2})=\frac{1}{2}[\psi(\frac{\mu+1}{2})-\psi(\frac{\mu}{2})]$, and $\Gamma(2\theta)\psi(2\theta)=\int_0^{\infty}d\tau\tau^{2\theta-1}e^{-\tau}\ln\tau$ with $\psi(y)$ denoting the Euler's psi function [32], we eventually obtain the intermediate time asymptote of $G(\mathbf{r},t)$ as

$$G(\mathbf{r},t)|_{1/r\gg k_c\gg 1/L}\approx A' r^{2m+2\rho+4m\theta-d}[A_0-\ln(k_c r)]+\sum_{l=1,l\neq\alpha}^{\infty}A_l k_c^{d-2m-2\rho-4m\theta}(k_c r)^{2l} \quad (31)$$

with the coefficients

$$A'=\frac{D'_{\rho}\Gamma(2\theta)(-1)^{1+m+\rho+2m\theta-d/2}}{2^{2m+2\rho+4m\theta-d}\Gamma\left(m+\rho+2m\theta-\frac{d}{2}+1\right)\Gamma(m+\rho+2m\theta)}, \quad (32)$$

$$A_0=\Omega-\frac{1}{2m}\left[\ln 2+\psi\left(\theta+\frac{1}{2}\right)\right], \quad (33)$$

and the value of the coefficient Ω given in Eq. (A2) of the Appendix. Note that the expression of the coefficient A_l is exactly identical to that for the cases with the exponent α being a noninteger, Eq. (25). Subsequently, by substituting the global roughness exponent $\alpha=m+\rho+2m\theta-d/2$, the dynamic exponent $z=2m$, and the characteristic wave-vector $k_c=(\nu t)^{-1/(2m)}$ into the above equation, the intermediate time asymptote of $G(\mathbf{r},t)$ is rewritten as

$$G(\mathbf{r},t)|_{L^z\gg\nu t\gg r^z}\approx A' r^{2\alpha}\left[\ln\left(\frac{(\nu t)^{1/z}}{r}\right)+A_0\right]+\sum_{l=1,l\neq\alpha}^{\infty}A_l(\nu t)^{2(\alpha-l)/z}r^{2l}. \quad (34)$$

In Eq. (34), the major qualitative difference from Eq. (27) is the appearance of the term $r^{2\alpha}\ln[(\nu t)^{1/z}/r]$, which is in-

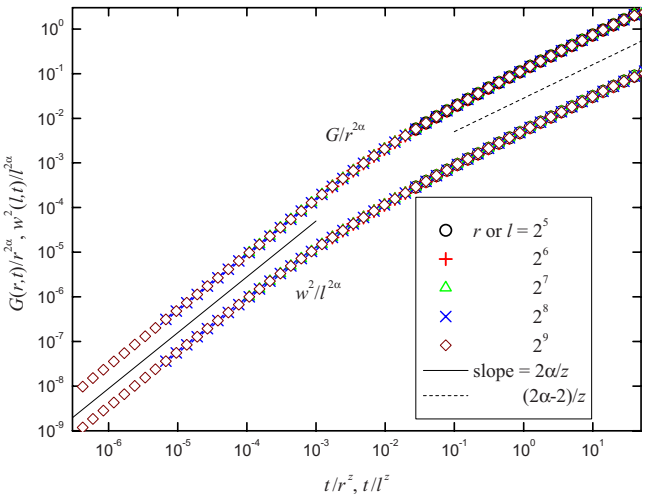

FIG. 2. (Color online) Data collapse of the scaling plot of $G(r,t)/r^{2\alpha}$ ($w^2(l,t)/l^{2\alpha}$) vs t/r^z (t/l^z) for the growth processes governed by Eq. (1) with the global roughness exponent $\alpha>1$. The data are generated with $m=2$, $d=2$, $(\rho,\theta)=(0.3,0.3)$, and the lateral linear size of the substrate $L=2^{13}$ sites. The solid and dashed straight lines with the slopes equal to $2\alpha/z$ and $2(\alpha-1)/z$ (with $\alpha=2.5$ and $z=4$), respectively, are drawn for a guide to the eyes.

deed the signature for the cases with the exponent α being an integer. Specifically, if the exponent $\alpha=1$, the most leading term in Eq. (34) is $r^2\ln[(\nu t)^{1/z}/r]$; if the exponent α is an integer larger than one, the terms $((\nu t)^{2(\alpha-1)/z}r^2,\cdots,(\nu t)^{2/z}r^{2(\alpha-1)},\ln[(\nu t)^{1/z}/r]r^{2\alpha})$ are all dominant over the term $r^{2\alpha}$ in Eq. (34). Recall that the correction term to scaling in equilibrium critical phenomena does not display a unique type of behavior; it can correspond to a logarithmic correction, to a cusplike correction, or even to a jump discontinuity. The above three types have all been observed in experimental measurements of specific heat or sound speed near the critical temperature [33]. Here, we rigorously and explicitly show that the dynamic scaling behaviors of the growth processes governed by Eq. (1) actually display logarithmic corrections if the global roughness exponent is an integer.

Regardless of the exponent α being an integer or not, the system with the exponent $\alpha>1$ displays anomalous dynamic scaling behaviors, compared with the generalized dynamic scaling ansatz Eq. (4). From the above analysis, we obtain the local roughness exponent $\alpha_{\rm loc}=1$ for the systems with the exponent $\alpha\geq 1$ and $\alpha_{\rm loc}=\alpha$ for the systems with the exponent $\alpha<1$. In addition, these anomalous terms (dominant over the term $r^{2\alpha}$) reveal local interfacial orientational instability, which will grow indefinitely with time in the thermodynamic limit (i.e., $L\to\infty$). For illustration, Fig. 2 shows the data collapse plot of $G(\mathbf{r},t)/r^{2\alpha}$ vs t/r^z in the early and intermediate time regimes for the growth processes governed by Eq. (1) with the exponent $\alpha>1$. In Fig. 2, the nonsaturation of $G(\mathbf{r},t)$ in the intermediate time regime manifests anomalous scaling behaviors and local interfacial orientational instability. The above result is independent of the individual values of the substrate dimensionality d, the noise correlation indices (ρ,θ), and the parameter m in Eq. (1). In the past literature, there have been several discussions on the value of the local roughness exponent. The authors of Ref. [34], by employing the Schwartz inequality, have shown $\alpha_{\rm loc}\leq 1$. In addition, the authors of Ref. [35], by applying the dynamical renormalization group analysis, have shown that $\alpha_{\rm loc}=1$ for the growth processes with white noise having the exponent $\alpha>1$. Here, we extend the above result to the growth processes with spatiotemporally correlated noise in arbitrary dimensions. Furthermore, the authors of Ref. [36] have argued that, for the (1+1)-dimensional interfaces, the structure factors $\tilde{h}(k,t)\tilde{h}(-k,t)$ always obey the ordinary dynamic scaling ansatz. Since the class of growth processes governed by Eq. (1) is exactly solvable, it offers a solid example for explicit calculation of the structure factors:

$$\overline{\tilde{h}(\mathbf{k},t)\tilde{h}(-\mathbf{k},t)}=\frac{D_\rho}{\nu k^{2m+2\rho}}\int_0^t d\tau(e^{-\nu k^{2m}\tau}-e^{-\nu k^{2m}(2t-\tau)})\tau^{2\theta-1}$$
$$=k^{-(2m+2\rho+4m\theta)}f(kt^{1/(2m)})=k^{-(2\alpha+d)}f(kt^{1/z}), \tag{35}$$

with $f(u)\sim$ contant for $u\gg 1$ and $f(u)\sim u^{2\alpha+d}$ for $u\ll 1$. Hence, for the growth processes governed by Eq. (1), the structure factor indeed always obeys the ordinary dynamic scaling ansatz, independent of the values of the exponent α and the substrate dimensionality d.

3. Late-time asymptote

The late-time regime is characterized by $k_c\ll 1/L$, which implies $\nu k_{\mathbf{n}}^{2m}t\gg 1$ for all $k_{\mathbf{n}\neq\mathbf{0}}$ in Eq. (10). Hence,

$$G(\mathbf{r},t)|_{k_c\ll 1/L}\approx\frac{2D_\rho\Gamma(2\theta)}{L^d\nu}\sum_{\mathbf{n}\neq\mathbf{0}}\frac{1-\cos(\mathbf{k_n}\cdot\mathbf{r})}{k_{\mathbf{n}}^{2m+2\rho+4m\theta}}. \tag{36}$$

For the 1+1 dimensional case, the above expression only involves a single sum and this summation can be exactly conducted by employing the appropriate formulas available in the mathematical handbook. Therefore, in Ref. [23], by using the following formula [32]:

$$\sum_{j=1}^{\infty}\frac{\cos(jx+y)}{j^a}=\frac{(2\pi)^a}{2\Gamma(a)\sin(a\pi)}\left[\sin\left(y+\frac{a\pi}{2}\right)\zeta\left(1-a,1-\frac{x}{2\pi}\right)-\sin\left(y-\frac{a\pi}{2}\right)\zeta\left(1-a,\frac{x}{2\pi}\right)\right]$$

with $\mathrm{Re}(a)>1$ and $0\leq x\leq 2\pi$, we expressed the late-time asymptote of $G(r,t)$ in 1+1 dimensions in terms of the generalized zeta function (Eq. (21) of Ref. [23]). Note that the equation below Eq. (21) of Ref. [23] (the mathematical relation among the generalized zeta functions) actually fails when β is an odd integer; hence, the derived results in Ref. [23] following this relation only work for the cases with the global roughness exponent being a noninteger. For the higher dimensional case, Eq. (36) involves the multiple sum. We have looked through many mathematical handbooks and cannot find the corresponding formulas to carry out this multiple sum. Thus, the procedure used in Ref. [23] cannot be applied to the general dimensional case. In order to obtain an explicit expression of the late-time asymptote of $G(\mathbf{r},t)$ in arbitrary dimensions, we decide to approximate the multiple sum by a

continuous multiple integral with a spherical hole of volume $(2\pi/L)^d$ around the origin. Consequently,

$$G(\mathbf{r},t)|_{k_c\ll 1/L} \approx \frac{4D_\rho\Gamma(2\theta)}{(2\pi)^d\nu^{1+2\theta}}\int_{k_0}^{\infty} k^{d-1-2m-2\rho-4m\theta}dk\Bigg\{\delta_{d,1}[1 - \cos(kr)] + (1-\delta_{d,1})\Bigg(\prod_{j=1}^{d-1}\int_0^{\pi}\sin^{d-1-j}\theta_j d\theta_j\Bigg) \times[1-\cos(kr\cos\theta_1)]\Bigg\}. \tag{37}$$

By employing the relations: $J_{-1/2}(y)=\sqrt{\frac{2}{\pi y}}\cos y$ and $\int_0^{\pi}\cos(y\cos x)\sin^{2\mu}xdx=\sqrt{\pi}(2/y)^{\mu}\Gamma(\mu+1/2)J_{\mu}(y)$, Eq. (37) can be recast as

$$G(\mathbf{r},t)|_{k_c\ll 1/L} \approx \frac{D'_\rho\Gamma(2\theta)}{\Gamma(d/2)}\int_{k_0}^{\infty} dk k^{d-1-2m-2\rho-4m\theta}\Bigg[1-\Gamma\left(\frac{d}{2}\right)\times\left(\frac{2}{kr}\right)^{d/2-1}J_{d/2-1}(kr)\Bigg]. \tag{38}$$

In the following, we will separately discuss the cases with the exponent α being a noninteger or an integer.

(i) For the cases with the exponent α being a noninteger:

By employing Eq. (19) and with some calculation, we obtain

$$G(\mathbf{r},t)|_{k_c\ll 1/L} \approx Cr^{2m+2\rho+4m\theta-d} + \sum_{l=1}^{\infty} C_l k_0^{d-2m-2\rho-4m\theta}(k_0r)^{2l} \tag{39}$$

with the coefficients

$$C = -\frac{D'_\rho\Gamma(2\theta)\Gamma(d/2-m-\rho-2m\theta)}{2^{2m+2\rho+4m\theta-d+1}\Gamma(m+\rho+2m\theta)} \tag{40}$$

and

$$C_l = \frac{(-1)^l D'_\rho\Gamma(2\theta)}{4^l(d-2m-2\rho-4m\theta+2l)\Gamma(d/2+l)l!}. \tag{41}$$

By substituting the global roughness exponent $\alpha=m+\rho+2m\theta-d/2$ and $k_0=2\sqrt{\pi}[\Gamma(d/2+1)]^{1/d}/L$ into the above equation, the late-time asymptote of $G(\mathbf{r},t)$ can then be rewritten as

$$G(\mathbf{r},t)|_{\nu t\gg L^z} \approx Cr^{2\alpha} + \sum_{l=1}^{\infty} C'_l L^{2(\alpha-l)}r^{2l}, \tag{42}$$

with the coefficients $C'_l=C_l\{2\sqrt{\pi}[\Gamma(d/2+1)]^{1/d}\}^{2(l-\alpha)}$. This result is generally applicable for arbitrary substrate dimension d. The coefficients in Eq. (23) of Ref. [23] can be recast in the same form as Eq. (42) in this paper, after taking the continuum limit in $\mathbf{k}$-space and employing the relations in Eq. (26). In Ref. [23], the term $\delta^{\beta-1}$ [in the equation below Eq. (21)] should be replaced by $-\delta^{\beta-1}$. Accordingly, the coefficient A in Eq. (22) of Ref. [23] should add a minus sign. Recall that the inverse of the characteristic wave-vector $1/k_c$ $[=(\nu t)^{1/z}]$ scales as the correlation length (of the height fluctuations) along the substrate space. For the late-time regime, the correlation length has reached the lateral linear size of the system. Hence, it is natural to have the form of Eq. (42) being similar to Eq. (27). It is just like the time t in the intermediate time asymptote of $G(\mathbf{r},t)$ being substituted by $O(L^z/\nu)$. For the system with the global roughness exponent $\alpha<1$, the leading term in Eq. (42) is $r^{2\alpha}$. In contrast, for the system with global roughness exponent $\alpha>1$, the leading terms $(L^{2(\alpha-1)}r^2,\cdots,L^{2(\alpha-[\alpha])}r^{2[\alpha]})$ are all dominant over the term $r^{2\alpha}$ in Eq. (42).

(ii) For the cases with the exponent α being an integer:

Recall that the mathematical formula Eq. (19) (given by Ref. [32]) actually fails when $\mu+\lambda$ being an odd negative integer. Hence, this mathematical formula is not applicable here. By employing Eq. (A1) (which we derive in the Appendix), the late-time asymptote of $G(\mathbf{r},t)$ is obtained as

$$\begin{aligned} G(\mathbf{r},t)|_{k_c\ll 1/L} &\approx \frac{(-1)^{1+\rho+2m\theta+m-d/2}D'_\rho\Gamma(2\theta)r^{2m+2\rho+4m\theta-d}}{2^{2m+2\rho+4m\theta-d}\Gamma(m+\rho+2m\theta)\Gamma(1+m+\rho+2m\theta-d/2)} \\ &\quad\times[\Omega-\ln(k_0r)] + \sum_{l=1,l\neq\alpha}^{\infty} k_0^{d-2m-2\rho-4m\theta}(k_0r)^{2l} \\ &\quad\times\left[\frac{(-1)^l D'_\rho\Gamma(2\theta)}{4^l(d-2m-2\rho-4m\theta+2l)\Gamma(d/2+l)l!}\right] \\ &= C'r^{2m+2\rho+4m\theta-d}[\Omega-\ln(k_0r)] \\ &\quad+\sum_{l=1,l\neq\alpha}^{\infty} C_l k_0^{d-2m-2\rho-4m\theta}(k_0r)^{2l}, \end{aligned} \tag{43}$$

with the value of the coefficient Ω given in Eq. (A2) of the Appendix. Again, by substituting the exponent $\alpha=m+\rho+2m\theta-d/2$ and $k_0=2\sqrt{\pi}[\Gamma(d/2+1)]^{1/d}/L$ into the above equation, the late-time asymptote of $G(\mathbf{r},t)$ can then be recast as

$$G(\mathbf{r},t)|_{\nu t\gg L^z} \approx C'r^{2\alpha}[\ln(L/r)+C_0] + \sum_{l=1,l\neq\alpha}^{\infty} C'_l L^{2(\alpha-l)}r^{2l} \tag{44}$$

with the coefficient $C_0=\Omega-\ln\{2\sqrt{\pi}[\Gamma(d/2+1)]^{1/d}\}$. In Eq. (44), the major qualitative difference from Eq. (42) is the appearance of the term $r^{2\alpha}\ln(L/r)$. If the exponent $\alpha=1$, the most leading term in Eq. (44) is $r^2\ln(L/r)$. If the exponent α is an integer larger than one, the terms $(L^{2(\alpha-1)}r^2,\ldots,L^2r^{2(\alpha-1)},\ln(L/r)r^{2\alpha})$ are all dominant over the term $r^{2\alpha}$ in Eq. (44). Hence, this logarithmic correction is indeed the signature difference from the cases with the exponent α being a noninteger.

Furthermore, the above explicit expressions of the asymptotes of $G(\mathbf{r},t)$ in successive time regimes indicate the following generic features for unstable surface growth: (a) the characteristic lateral linear size of hills (or valleys) grows with time according to $(\nu t)^{1/z}$, with $z=2m$ being an even positive integer. Since m is a decreasing step function of temperature, the lateral size of hills (or valleys) will develop slower in time if one lowers the substrate temperature. (b) The measure of average local inclination of hills (or valleys)

scales to $[G(r,t)^{1/2}/r]_{r\ll(\nu t)^{1/z}\ll L}$. Accordingly, its value increases in time with the leading power-law exponents $\{\frac{1}{2}+\theta-\frac{i+d/2-\rho}{2m};i=1,2,\ldots,[\alpha]\}$. All these exponents are increasing functions of m, ρ, and θ. However, recall that m is a decreasing step function of growth temperature while the noise correlation indices (ρ,θ) are increasing functions of both the deposition flux and the growth temperature. Hence, it implies that, if one lowers the substrate temperature, the magnitude of local inclination of hills (or valleys) may grow either faster or slower in time, which depends on materials and substrate crystalline planes. On the contrary, the local inclination of hills (or valleys) will definitely develop more quickly in time, if one enhances the deposition flux. (c) The dimensionality d has minor effect on the lateral development of hills or valleys (only through the parameter ν). In contrast, the dimensionality d has stronger influence on the temporal development of local inclination of hills (or valleys). More specifically, all the temporal leading exponents are decreasing functions of d. (d) As the value of m increases, the influence of d and ρ on the temporal development of local orientational instability will be weakened, while the influence due to θ remains unaltered. This characteristic is especially important for electrochemical deposition, since it is well known that the noise in electrochemical deposition is strongly temporally correlated [5]. Remarkably, the above derived characteristics of unstable surface growth are in excellent agreement with various experimental observations in the literature, ranging from electrochemical deposition to molecular-beam epitaxy for many different materials [5,10,12–15]. Here, we have succeeded in giving these experimental observations a unified picture through the phenomenological growth equation Eq. (1) and the analysis of $G(\mathbf{r},t)$.

B. Slope-slope correlation function

Note that the most renowned feature of unstable surface growth is the formation of macroscopic structures. Since the slope-slope correlation function $S(\mathbf{r},t)$ is aimed to quantitatively characterize the correlation between the slopes at different sites, one naturally expects there should exist some signature difference in $S(\mathbf{r},t)$ between stable surface growth and unstable surface growth. Therefore, in this subsection, a detailed investigation on the behavior of $S(\mathbf{r},t)$ will be undertaken, including the asymptotic behavior in various time regimes, the qualitative difference in the functional shape of $S(\mathbf{r},t)$ between different categories of surface growth, and the quality of determining the dynamic exponent z by using the first zero of $S(\mathbf{r},t)$.

The slope-slope correlation function is defined as

$$S(\mathbf{r},t) \equiv \overline{\langle \nabla h(\mathbf{x},t)\cdot\nabla h(\mathbf{x}+\mathbf{r},t)\rangle_L} = -\nabla^2[\overline{\langle h(\mathbf{x},t)h(\mathbf{x}+\mathbf{r},t)\rangle_L}]$$
$$= \frac{1}{2}\nabla^2 G(\mathbf{r},t). \tag{45}$$

For systems obeying dynamic scaling $G(r,t)=t^{2\alpha/z}f(r/t^{1/z})$, we obtain $S(r,t)=t^{2(\alpha-1)/z}g(r/t^{1/z})$ by using the relation $S(\mathbf{r},t)=\frac{1}{2}\nabla^2 G(\mathbf{r},t)$. Hence, the first zero of $S(r,t)$, $r_0(t)$, is exactly proportional to $t^{1/z}$ without any approximation if the lateral linear size of the substrate $L\to\infty$. Note that this relation is exact, not just the asymptotic behavior. For a system with finite L, we derive $r_0(t)\propto t^{1/z}$ in the range of the correlation length much less than L. Once the correlation length reaches the order of L, the finite-size effect enters and restricts the increase of $r_0(t)$ with time. Eventually, $r_0(t)$ saturates. If the crossover regime (from $t^{1/z}$ to saturation) is very narrow, then this method of determining the dynamic exponent z based on $r_0(t)$ will be superior to other methods in the

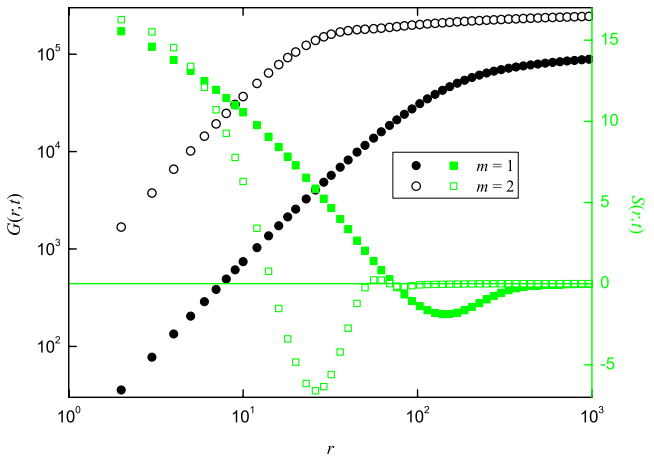

FIG. 3. (Color online) The plot of $G(r,t)$ (circles) and $S(r,t)$ (squares) vs r in the log-log scale and the linear-log scale, respectively. The substrate dimension $d=1$, the lateral linear size of the substrate $L=2^{15}$ sites, and the time $t=2^{12}$ time steps. The noise correlation indices $(\rho,\theta)=(0.3,0.2)$ and the parameters ν and D_ρ are set to be 1. The solid and hollow symbols correspond to the cases governed by Eq. (1) with $m=1$ and 2, respectively. Note that the values of $S(r,t)$ shown in the figure for the case with $m=2$ have been reduced by a factor of 50 for visual clarity.

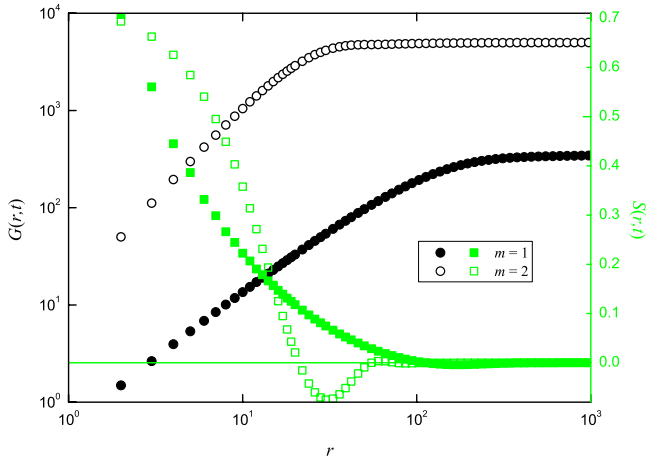

FIG. 4. (Color online) The plot of $G(r,t)$ (circles) and $S(r,t)$ (squares) vs r in the log-log scale and the linear-log scale, respectively. The substrate dimension $d=2$, the lateral linear size of the substrate $L=2^{15}$ sites, and the time $t=2^{12}$ time steps. The noise correlation indices $(\rho,\theta)=(0.3,0.2)$ and the parameters ν and D_ρ are set to be 1. The solid and hollow symbols correspond to the cases governed by Eq. (1) with $m=1$ and 2, respectively. Note that the values of $S(r,t)$ shown in the figure for the case with $m=2$ have been reduced by a factor of 70 for visual clarity.

literature, due to its precise definition and objectivity.

The generic properties of $S(r,t)$ are obtained as follows: (a) $S(r,t)>0$ in the range of $r<r_0(t)$. (b) $S(r,t)\sim 0$ as $r\to\infty$. (c) For the interfaces obeying dynamic scaling $G(r,t)=t^{2\alpha/z}f(r/t^{1/z})$, $r_0(t)$ is almost perfectly proportional to $t^{1/z}$ in the range of $r_0(t)$ much less than the lateral linear size of the substrate. For illustration, Figs. 3 and 4 show the plots of $G(r,t)$ (circles) and $S(r,t)$ (squares) vs r in the log-log and linear-log scales at a fixed time, for the substrate dimension $d=1$ and 2, respectively. The solid and hollow symbols (in Figs. 3 and 4) correspond to the cases governed by Eq. (1) with $m=1$ and 2, respectively. The details of other parameter values are given in the figure captions. Both figures clearly demonstrate the generic behavior of $S(r,t)$ mentioned above, independent of the substrate dimensionality and the roughness exponent. As shown in the figures, the values of $S(r,t)$ sharply drop down as $G(r,t)$ goes from the power-law scaling ($r^{2\alpha_{\rm loc}}$) regime to saturation. Indeed, using $r_0(t)$ to characterize the correlation length is very appropriate due to its quantitatively precise definition.

Next, by following the derivation of $G(r,t)$ in Sec. II A, the asymptotes of $S(r,t)$ for the three successive time regimes are obtained as follows.

(i) For the cases with the global roughness exponent α being a noninteger:

$$S(r,t)\approx\begin{cases}0, & \text{for } \nu t\ll r^z,\\ \tilde{A}r^{2\alpha-2}+\sum_{p=1}^{\infty}\tilde{A}_p(\nu t)^{2(\alpha-p)/z}r^{2p-2}, & \text{for } r^z\ll \nu t\ll L^z,\\ \tilde{C}r^{2\alpha-2}+\sum_{p=1}^{\infty}\tilde{C}_pL^{2\alpha-2p}r^{2p-2}, & \text{for } \nu t\gg L^z.\end{cases}\tag{46}$$

(ii) For the cases with the global roughness exponent α being an integer:

$$S(r,t)\approx\begin{cases}0, & \text{for } \nu t\ll r^z,\\ \tilde{A}'r^{2\alpha-2}\left[\ln((\nu t)^{1/z}/r)+A_0-\frac{4\alpha+d-2}{2\alpha(2\alpha+d-2)}\right]+\sum_{p=1,p\neq\alpha}^{\infty}\tilde{A}_p(\nu t)^{2(\alpha-p)/z}r^{2p-2}, & \text{for } r^z\ll \nu t\ll L^z,\\ \tilde{C}'r^{2\alpha-2}\left[\ln(L/r)+C_0-\frac{4\alpha+d-2}{2\alpha(2\alpha+d-2)}\right]+\sum_{p=1,p\neq\alpha}^{\infty}\tilde{C}_pL^{2\alpha-2p}r^{2p-2}, & \text{for } \nu t\gg L^z.\end{cases}\tag{47}$$

The coefficients are derived as $\tilde{A}=\alpha(2\alpha+d-2)A$, $\tilde{A}'=\alpha(2\alpha+d-2)A'$, $\tilde{C}=\alpha(2\alpha+d-2)C$, $\tilde{C}'=\alpha(2\alpha+d-2)C'$, $\tilde{A}_p=p(2p+d-2)A_p$, and $\tilde{C}_p=p(2p+d-2)C_p$. For stable surface growth (corresponding to the exponent $\alpha<1$), the slope-slope correlation function quickly reaches saturation in time and its most leading term is proportional to $r^{2\alpha-2}$. For the growth process with the exponent $\alpha=1$, the most leading terms of $S(r,t)$ in the intermediate and late-time regimes are $\ln[(\nu t)^{1/z}/r]$ and $\ln(L/r)$, respectively. Again, we obtain a logarithmic correction at the border between stable and unstable surface growth. In contrast, for unstable surface growth, the slope-slope correlation grows with time (in a power-law form) indefinitely in the thermodynamic limit $L\to\infty$. More specifically, for unstable surface growth with the exponent α being a non-integer larger than one, the terms $((\nu t)^{2(\alpha-1)/z}\cdots,(\nu t)^{2(\alpha-[\alpha])/z}r^{2[\alpha]-2})$ in the intermediate time regime and the terms $(L^{2(\alpha-1)},\cdots,L^{2(\alpha-[\alpha])}r^{2[\alpha]-2})$ in the late-time regime are dominant over the term $r^{2\alpha-2}$; for unstable surface growth with the exponent α being an integer larger than one, the terms $\{(\nu t)^{2(\alpha-1)/z},\cdots,(\nu t)^{2/z}r^{2(\alpha-2)},\ln[(\nu t)^{1/z}/r]r^{2(\alpha-1)}\}$ in the intermediate time regime and the terms $[L^{2(\alpha-1)},\cdots,L^2r^{2(\alpha-2)},\ln(L/r)r^{2(\alpha-1)}]$ in the late-time regime are dominant over the term $r^{2\alpha-2}$.

Notably, we obtain that the functional shapes of $S(r,t)$ are distinctly different for stable surface growth and unstable surface growth. Specifically, in the region of $r<r_0(t)$, $S(r,t)$ is a convex function of r for the growth process with the exponent $\alpha<1$. On the contrary, for the growth process with the exponent $\alpha>1$, $S(r,t)$ is independent of r in the region of $r\ll r_0(t)$ and sharply drops to zero as r is close to $r_0(t)$; this distinguished functional shape indicates that there exists a considerable degree of order in the slope-slope correlation within the spatial range characterized by $r_0(t)$ and this ordering gradually develops from a short-range order to a long-range order, as $r_0(t)$ increases with time according to $r_0(t)\sim t^{1/z}$. In addition, the lateral linear length scale of the macroscopic hill (or valley) can also be characterized by $r_0(t)$. Note that this qualitative behavior of unstable surface growth is very similar to phase separation in a binary alloy at low temperature, by mapping the values of positive h and negative h (at the comoving reference frame with average advancing velocity) to the concentrations of type A and type B metals in a binary alloy.

For illustration, Figs. 5(a) and 5(b) demonstrate the data collapse plots of $S(r,t)/t^{2(\alpha-1)/z}$ vs $r/t^{1/z}$ for the growth process governed by Eq. (1) with the exponent $\alpha<1$ and $\alpha>1$, respectively. In Fig. 5, data sets are generated with the substrate dimension $d=2$, the noise correlation indices $(\rho,\theta)=(0.3,0.2)$, but the parameter $m=1$ and 2 [for (a) and

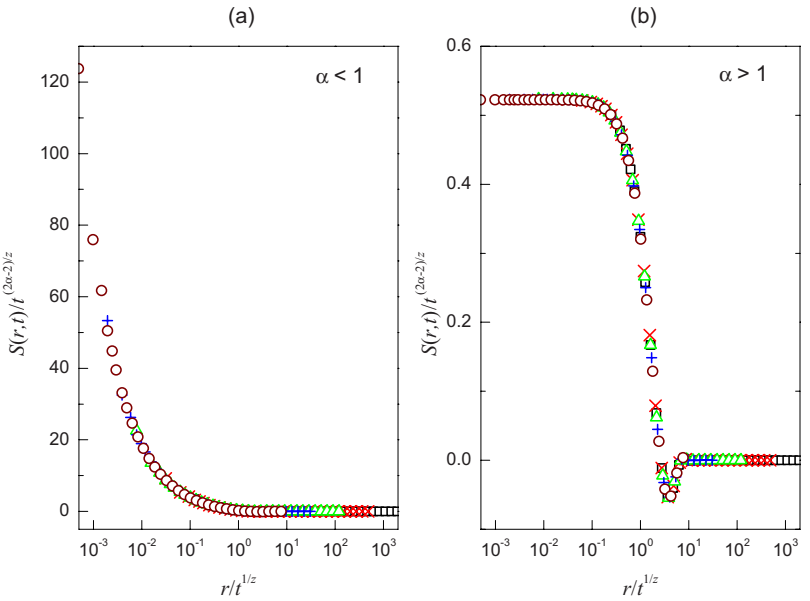

FIG. 5. (Color online) Data collapse of the scaling plot of $S(r,t)/t^{2(\alpha-1)/z}$ vs $r/t^{1/z}$ for the growth processes governed by Eq. (1) with the global roughness exponent (a) $\alpha<1$ and (b) $\alpha>1$. Data sets are generated with the substrate dimension $d=2$, the noise correlation indices $(\rho,\theta)=(0.3,0.2)$, but the parameter $m=1$ and 2 [for (a) and (b), respectively]. Accordingly, the exponents $(\alpha,z)=(0.7,2)$ for (a) and the exponents $(\alpha,z)=(2.1,4)$ for (b). The successive time slices for data collapse are $t=[2^6(\square),2^{10}(\times),2^{14}(\triangle),2^{18}(+),2^{22}(\bigcirc)]$ time steps for (a) and $t=[2^{12}(\square),2^{20}(\times),2^{28}(\triangle),2^{36}(+),2^{44}(\bigcirc)]$ time steps for (b).

(b), respectively]. Accordingly, the exponents $(\alpha,z)=(0.7,2)$ for Fig. 5(a) and the exponents $(\alpha,z)=(2.1,4)$ for Fig. 5(b). Remarkably, we find that this distinct feature of $S(r,t)$ (as shown in Fig. 5) is independent of the substrate dimensionality and other details of growth mechanism. The only relevant factor is the value of the exponent α less than or greater than one. It is indeed a signature difference between stable surface growth and unstable surface growth. Experimentally, one usually uses the quantitative measurement of the exponent α to classify experimental systems into the categories of stable surface growth or unstable surface growth. However, for the experimental systems close to the border line, the method of classification based on the measured value of α may cause criticism since any quantitative determination of the value of the exponent α certainly contains some degree of uncertainty. Hence, the distinctly different functional shapes of $S(r,t)$ for stable surface growth and unstable surface growth are especially useful for settling this controversy. Note that all these numerical calculations of $G(r,t)$ and $S(r,t)$ (with arbitrary values of r, t, L, and substrate dimension) are performed according to an efficient algorithm, which will be explained in detail in the next section.

Subsequently, let us move on to numerically investigate the behavior of $r_0(t)$. As mentioned earlier in this subsection, the excellency of determining the dynamic exponent z based on $r_0(t)$ strongly depends on whether the range of the crossover regime is very narrow. We numerically find that, for the growth process governed by Eq. (1), the crossover regime of $r_0(t)$ is extremely short and, hence, the power law fitting to $t^{1/z}$ is excellent. For illustration, Fig. 6 shows the log-log plot of $r_0(t)$ vs time t, with the parameter m in Eq. (1) being 1 or 2, the substrate dimensionality d equal to 1 or 2, and the noise correlation indices $(\rho,\theta)=(0.3,0.2)$. The lateral linear size of the substrate L is equal to 2^{15} (=32 768) sites. Recall that the dynamic exponent $z=2m$ and the global roughness exponent $\alpha=m+\rho+2m\theta-d/2$. In Fig. 6, the corresponding exponents are $(\alpha,z)=(1.2,2)$, (0.7,2), (2.6,4), and (2.1,4) for the cases with $(d,m)=(1,1)$, (2,1), (1,2), and (2,2), respectively. Figure 6 clearly reveals that the saturation value of $r_0(t)$ is larger than $L/5$ and the crossover regime is so narrow that the power law fitting is almost perfect even if $r_0(t)$ reaches half of its saturation value. Therefore, we conclude that this method of determining the dynamic exponent z based on $r_0(t)$ gives very convincing results for the growth process governed by Eq. (1).

In the literature, there are two conventional methods for measuring the dynamic exponent z. The first method is to adjust the value of z until the best data collapse of the scaling plot of $G(r,t)$ [or $w(l,t)$] is obtained. However, for some physical systems, a certain range of the value of z may produce equally-good data collapse of the scaling plot and, hence, this method does not give very precise estimate of the

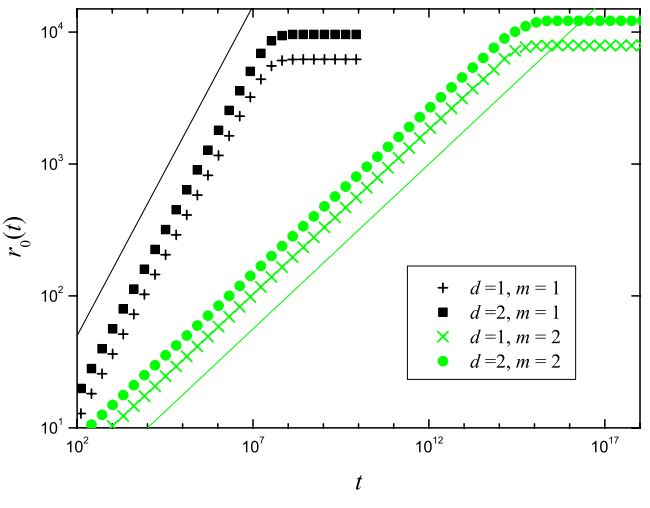

FIG. 6. (Color online) The log-log plot of the first zero $r_0(t)$ of the slope-slope correlation function vs time t, for the growth processes governed by Eq. (1) with the noise correlation indices $(\rho,\theta)=(0.3,0.2)$. The plus, square, cross, and circle symbols correspond to the cases with the substrate dimension d and the parameter m in Eq. (1) equal to (1,1), (2,1), (1,2), and (2,2), respectively. The parameters ν and D_ρ are set to be 1. The lateral linear size of the substrate $L=2^{15}$ sites. The straight lines with the slope 0.5 (for $m=1$) or 0.25 (for $m=2$) are drawn for a guide to the eyes.

value of z. The scheme of the second method is as follows. For the interfacial width of the physical system obeying power-law scaling, the characteristic length $l_c(t)$ at a given time t is defined as $w^2(l_c,t)=aw^2(L,t)$, with a being a constant between 0 and 1. For the interfacial width of the physical system obeying logarithmic scaling, the characteristic length $l_c(t)$ is defined as $w^2(l_c,t)=w^2(L,t)-b$, with b being a positive constant. Typically, the values of a and b are chosen such that $l_c>10$ and $l_c \ll L$. Then the value of the dynamic exponent z is determined by $l_c \propto t^{1/z}$. The drawback of this method is that one first needs to assume power-law scaling or logarithmic scaling in order to use the appropriate formula for determining l_c. In addition, this method allows one to freely choose the value of the constant a (or b) and, hence, may cause criticism if one is dealing with a physical system whose universality class is controversial.

In contrast, the method of determining the dynamic exponent z, based on the first zero of the slope-slope correlation function, has merits of precision and objectivity at the same time. To show the excellency of this statistical method in measuring the dynamic exponent z, we simulate the Das Sarma and Tamborenea (DT) model [37] in 2+1 dimensions. This model is a discrete solid-on-solid model with instantaneous relaxation and limited mobility, describing MBE growth under random deposition for certain temperature ranges. The growth rules of the DT model are defined as follows: (a) randomly choose a column j, and the incident adatom sticks at the top of column j if it has one or more lateral nearest neighbors at that position. (b) Otherwise, the nearest neighboring columns are tested. If the top positions of all these columns do not have lateral nearest neighbors, the incident adatom still sticks at the top of column j. If the top positions of one or more nearest neighboring columns have at least one lateral nearest neighbor, the incident adatom will deposit at the top of one of them with equal probability. In spite of the simple deposition and relaxation rules, the universality class of the DT model in 2+1 dimensions has remained controversial.

We first briefly review the debate on the universality class of the DT model in the literature. Early extensive simulations [28,38] on the 1+1 dimensional DT model produce the scaling exponents being approximately described by the MWV equation with white noise (with the additional complication of the qth order height difference correlation function displaying spatial multiscaling, indicating that the continuous description of the DT model is more complicated). Subsequently, theoretical studies [39,40] based on the Fokker-Planck approximation of the master equation with certain choice of regularization scheme predict that the 1+1 dimensional DT model is described by the Villain-Lai-Das Sarma (VLDS) growth equation [41] with white noise

$$\frac{\partial h(\mathbf{x},t)}{\partial t} = -\nu \nabla^4 h(\mathbf{x},t) + \lambda \nabla^2 |\vec{\nabla} h(\mathbf{x},t)|^2 + \eta(\mathbf{x},t). \quad (48)$$

By employing the noise reduction technique, Das Sarma *et al.* [42] numerically verify that the 1+1 dimensional DT model is asymptotically described by the VLDS equation with white noise, but they surprisingly find that the 2+1 dimensional DT model belongs to the universality class of the EW equation with white noise. Indeed, the determination of the universality class of the 2+1 dimensional DT model is a very subtle issue. Note that the scaling exponents of the EW equation with white noise in 2+1 dimensions are $\alpha=\alpha_{\mathrm{loc}}=0$ (logarithmic scaling), $\beta=0$, and $z=2$. The scaling exponents of the MWV equation with white noise in 2+1 dimensions are $\alpha=\alpha_{\mathrm{loc}}=1$ (power-law scaling with logarithmic correction), $\beta=1/4$, and $z=4$. The scaling exponents of the VLDS equation with white noise in 2+1 dimensions are $\alpha=\alpha_{\mathrm{loc}}=2/3$ (power-law scaling), $\beta=1/5$, and $z=10/3$. The authors of Ref. [43] find that the value of the dynamic exponent z of the 2+1 dimensional DT model is approximately consistent with the result of the EW equation with white noise, if one assumes the logarithmic scaling of the interfacial width; on the other hand, by assuming the power-law scaling of the interfacial width, the measured value of the dynamic exponent z of the 2+1 dimensional DT model in Ref. [43] is quite close to the result of the VLDS equation with white noise.

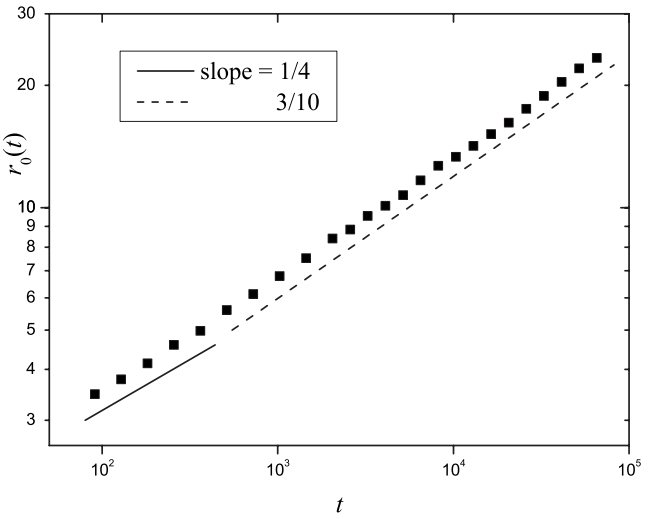

FIG. 7. A log-log plot of $r_0(t)$ [the first zero of $S(r,t)$] vs time t for the DT model with the substrate dimension $d=2$. The lateral size of the system is 1024×1024 lattice sites. The straight lines with the slope equal to 1/4 (solid) or 3/10 (dashed) are drawn for a guide to the eyes.

Since the method of determining the dynamic exponent z, based on the first zero $r_0(t)$ of the slope-slope correlation function, does not require any assumption on the logarithmic scaling (or the power-law scaling) of the interfacial width and no free parameters are included, this method is perfect for resolving the above controversy. We simulate the DT model in 2+1 dimensions with the maximum simulation time $T=2^{16}$ monolayers. The lateral size of the system is 1024×1024 sites and the periodic boundary condition is imposed. The number of realizations is 157 runs. In calculating $S(r,t)$, we first take self-average over the whole system and then take average over realizations. Figure 7 is the log-log plot of $r_0(t)$ [the first zero of $S(r,t)$] versus time t. Note that, in Eq. (48), the competition between the terms $\nabla^4 h$ and $\nabla^2|\vec{\nabla} h|^2$ produces a characteristic lateral length scale L^* (determined by ν/λ), which separates two scaling regimes with different scaling exponents. If the correlation length of the

system at time t is much smaller than L^*, the term $\nabla^4 h$ determines the scaling behavior and the dynamic exponent is given as $z=4$ (the MWV behavior). If the correlation length of the system at time t is much larger than L^*, the term $\nabla^2|\vec{\nabla}h|^2$ determines the scaling behavior and the dynamic exponent is given as $z=10/3$ (the VLDS behavior). As we have mentioned earlier in this subsection, $r_0(t)$ is a quantitative measure of the correlation length of the system at time t. In Fig. 7, the results clearly show that the reciprocal of the dynamic exponent $[1/z=\frac{\log[r_0(t_1)/r_0(t_2)]}{\log(t_1/t_2)}]$ indeed changes from 1/4 (the MWV behavior) to 3/10 (the VLDS behavior). Thanks to the excellency of determining the exponent z based on $r_0(t)$, our numerical results strongly support the argument that the best continuum description of the DT model is the VLDS equation. In conclusion, all the above simulation results strongly indicate that one should adopt this method first in determining the dynamic exponent z from experimental data.

C. Local interfacial width

The local interfacial widths is defined as

$$w^2(l,t) \equiv \overline{\langle\langle[h(\mathbf{x},t)-\langle h(\mathbf{x},t)\rangle_l]^2\rangle_l\rangle_L}, \tag{49}$$

with $\langle\cdots\rangle_l$ denoting the spatial average calculated within a d-dimensional local window of side length l throughout this paper. With some calculation, we obtain the exact relation between the square of the local interfacial width and the equal-time height difference correlation function as

$$w^2(l,t) = \left[\prod_{i=1}^{d}\frac{2}{l^2}\int_0^l dr_i(l-r_i)\right]\frac{1}{2}G(\mathbf{r},t). \tag{50}$$

By going through the similar derivation of $G(\mathbf{r},t)$, the asymptotes of $w^2(l,t)$ in the three successive time regimes are obtained as follows.

(i) For the cases with the global roughness exponent α being a noninteger:

$$w^2(l,t) \approx \begin{cases} O\left(\dfrac{D_\rho}{\nu^{(d-2\rho)/z}}t^{2\alpha/z}\right), & \text{for } \nu t \ll l^z, \\ \hat{A}l^{2\alpha}+\displaystyle\sum_{q=1}^{\infty}\hat{A}_q(\nu t)^{2(\alpha-q)/z}l^{2q}, & \text{for } l^z \ll \nu t \ll L^z, \\ \hat{C}l^{2\alpha}+\displaystyle\sum_{q=1}^{\infty}\hat{C}_q L^{2\alpha-2q}l^{2q}, & \text{for } \nu t \gg L^z. \end{cases} \tag{51}$$

(ii) For the cases with the global roughness exponent α being an integer:

$$w^2(l,t) \approx \begin{cases} O\left(\dfrac{D_\rho}{\nu^{(d-2\rho)/z}}t^{2\alpha/z}\right), & \text{for } \nu t \ll l^z, \\ \hat{A}' l^{2\alpha}[\ln((\nu t)^{1/z}/l)+A_0]+\displaystyle\sum_{q=1,q\neq\alpha}^{\infty}\hat{A}_q(\nu t)^{2(\alpha-q)/z}l^{2q}, & \text{for } l^z \ll \nu t \ll L^z, \\ \hat{C}' l^{2\alpha}[\ln(L/l)+C_0]+\displaystyle\sum_{q=1,q\neq\alpha}^{\infty}\hat{C}_q L^{2\alpha-2q}l^{2q}, & \text{for } \nu t \gg L^z. \end{cases} \tag{52}$$

For the growth process with the global roughness exponent $\alpha<1$, the most leading term of the asymptotes of $w^2(l,t)$ in the intermediate and late-time regimes is $l^{2\alpha}$. For the growth process with the exponent $\alpha=1$, the most leading terms of the asymptotes of $w^2(l,t)$ in the intermediate and late-time regimes are $l^2\ln((\nu t)^{1/z}/l)$ and $l^2\ln(L/l)$, respectively. Subsequently, for the growth process with the global roughness exponent being a non-integer larger than one, the anomalous terms $((\nu t)^{2(\alpha-1)/z}l^2,\ldots,(\nu t)^{2(\alpha-[\alpha])/z}l^{2[\alpha]})$ in the intermediate time regime and the anomalous terms $(L^{2(\alpha-1)}l^2,\ldots,L^{2(\alpha-[\alpha])}l^{2[\alpha]})$ in the late-time regime are dominant over the ordinary dynamic scaling term $l^{2\alpha}$; while for the exponent α being an integer larger than one, the anomalous terms $((\nu t)^{2(\alpha-1)/z}l^2,\ldots,(\nu t)^{2/z}l^{2(\alpha-1)},\ln((\nu t)^{1/z}/l)l^{2\alpha})$ in the intermediate time regime and the anomalous terms $[L^{2(\alpha-1)}l^2,\ldots,L^2l^{2(\alpha-1)},\ln(L/l)l^{2\alpha}]$ in the late-time regime are dominant over the ordinary dynamic scaling term $l^{2\alpha}$.

Indeed, the asymptotes of $w^2(l,t)$ bear the same form as those of $G(r,t)$ by simply substituting r in Eqs. (27), (34), (42), and (44) with $O(l)$. For illustration, Fig. 2 shows the data collapse in the scaling plot of $G(r,t)/r^{2\alpha}$ and $w^2(l,t)/l^{2\alpha}$ vs t/r^z and t/l^z, respectively, in the early and intermediate time regimes for the growth process governed by Eq. (1) with the exponent $\alpha>1$. The substrate dimensionality $d=2$ and the lateral linear size of the substrate $L=2^{13}$ sites. Figure 2 clearly shows the nonsaturation of $G(r,t)/r^{2\alpha}$ and $w^2(l,t)/l^{2\alpha}$ in the intermediate time regime, which manifests the property of local interfacial orientational instability. Moreover, Fig. 2 reveals an interesting phenomenon: The temporal span of crossover from the early time regime to the intermediate time regime is very long. This is exactly the issue raised in Ref. [43]: for a system consisting of long crossover behavior, the traditional method of measuring the scaling exponent is greatly influenced by the interval which one chooses for the power-law fit in the scaling plot. Hence,

we use a different method to determine the scaling exponent, based on the $[Q]$-th degree residual local interfacial widths. In the final part of this subsection, we will discuss this method in detail.

We will now focus on the unstable surface growth processes. Recall that such growth processes will gradually develop the macroscopic hills and/or valleys as growth time increases. Eventually, the effect of finite lateral system size enters and restricts further development of these macroscopic structures. From the viewpoint of industrial applications, the macroscopic structure of interface morphology and the local roughening properties are equally important. Since the pattern formation due to unstable surface growth may provide a new pathway for technological device design, it is essential to separately discuss the macroscopic structures and the residual interface width in a systematical way. So we first systematically express the macroscopic structure of the interface configuration in terms of Legendre polynomials order by order. Such an explicit and systematical expression can greatly help further study on the interface morphology. Let the $\{q\}$-th degree $[\{q\} \equiv (q_1, \ldots, q_d)]$ polynomial $\hat{h}_{\{q\}}(\mathbf{x},t)$ represent the macroscopic structure of the interface configuration within a d-dimensional observation window of side length l and centered at $\hat{\mathbf{x}}$,

$$\hat{h}_{\{q\}}(\mathbf{x},t) = \sum_{\{n\}=\{0\}}^{\{q\}} C_{\{n\}}(t) \prod_{j=1}^{d} P_{n_j}\left(\frac{2(x_j - \hat{x}_j)}{l}\right), \tag{53}$$

where the summation runs over the set of indices $0 \le n_i \le q_i$ for all $1 \le i \le d$ and $P_i(x)$ denotes the Legendre polynomial satisfying the orthogonal property $\int_{-1}^{1} dx P_i(x) P_{i'}(x) = 2\delta_{i,i'}/(2i+1)$. The adjustable parameters $C_{\{n\}}(t)$ are determined by the minimization of $\langle [h(\mathbf{x},t) - \hat{h}_{\{q\}}(\mathbf{x},t)]^2 \rangle_l$, which leads to

$$C_{\{n\}}(t) = \left\langle h(\mathbf{x},t) \prod_{j=1}^{d} (2n_j + 1) P_{n_j}\left(\frac{2(x_j - \hat{x}_j)}{l}\right) \right\rangle_l. \tag{54}$$

Note that the above expression is exact and completely general, applicable to any fluctuating systems in arbitrary dimensions.

In the ensuing analysis, we adopt the symbol $[Q]$ to denote the set of indices $\{n\} \equiv (n_1, \ldots, n_d)$ with $|\{n\}| \equiv \Sigma_{i=1}^{d} n_i \le Q$ and all n_i being nonnegative integers. Then, the $[Q]$-th degree residual local interfacial width within a d-dimensional observation window is defined as

$$w^2[Q](l,t) \equiv \overline{\langle \langle [h(\mathbf{x},t) - \hat{h}[Q](\mathbf{x},t)]^2 \rangle_l \rangle_L}, \tag{55}$$

where $\hat{h}[Q](\mathbf{x},t)$ $[= \Sigma_{|\{n\}| \le Q} \langle h(\mathbf{x},t) \Pi_{j=1}^{d} (2n_j + 1) P_{n_j}(\frac{2(x_j - \hat{x}_j)}{l}) \rangle_l \Pi_{j=1}^{d} P_{n_j}(\frac{2(x_j - \hat{x}_j)}{l})]$ represents the $[Q]$-th degree macroscopic structure of the interface morphology. With some complicated calculation, the exact and explicit relation between the $[Q]$-th degree residual local interfacial width and the equal-time height difference correlation function is obtained as:

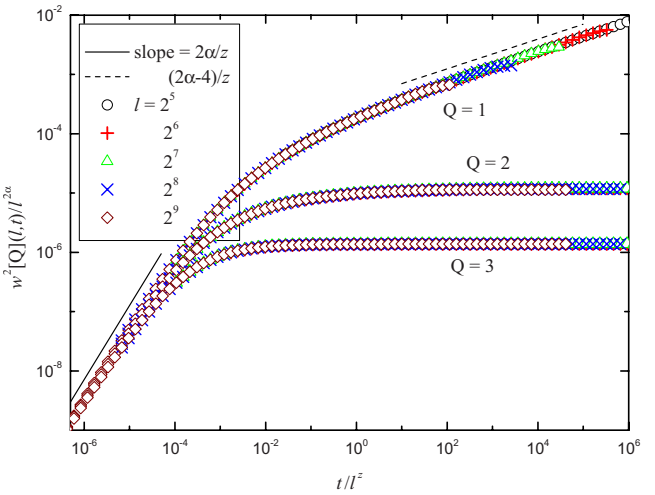

FIG. 8. (Color online) Data collapse of the scaling plot of the $[Q]$-th degree residual local interfacial width $w^2[Q](l,t)/l^{2\alpha}$ vs t/l^z, for the growth processes governed by Eq. (1) with the global roughness exponent $\alpha = 2.5$ and the dynamic exponent $z = 4$. The data are generated with the parameter $m = 2$, the substrate dimension $d = 2$, the noise correlation indices $(\rho, \theta) = (0.3, 0.3)$, and the lateral linear size of the substrate $L = 2^{13}$ sites. The straight lines with the slope equal to $2\alpha/z$ or $(2\alpha - 4)/z$ are drawn for a guide to the eyes.

$$w^2[Q](l,t) = \frac{1}{2} \prod_{j=1}^{d} \left(\frac{1}{l^2} \int_0^l dr_j \right) G(\mathbf{r},t) K[Q](\mathbf{r}) \tag{56}$$

with the kernel $K[Q](\mathbf{r})$ given by

$$K[Q](\mathbf{r}) = \sum_{|\{n\}| \le Q} \left\{ \prod_{j=1}^{d} \left[2(2n_j + 1) \times \int_{-l/2}^{l/2 - r_j} dx_j P_{n_j}\left(\frac{2x_j}{l}\right) P_{n_j}\left(\frac{2x_j + 2r_j}{l}\right) \right] \right\}. \tag{57}$$

For self-containedness, we list Eqs. (54)–(57), which have been rigorously derived by us in Ref. [44]. See Ref. [44] for the details of derivation.

Clearly, the design of the $[Q]$-th degree residual local interfacial width is to explore the scaling behavior of the surface fluctuation relative to macroscopic structures order by order. For illustration, Fig. 8 shows the data collapse of the scaling plot $w^2[Q](l,t)/l^{2\alpha}$ vs t/l^z for the growth processes governed by Eq. (1) with the global roughness exponent $\alpha = 2.5$. Theoretically, the second degree residual local interfacial width should be sufficient to suppress the leading anomalous terms and retrieve the ordinary dynamic scaling ansatz, i.e., reaching saturation in both the intermediate and late-time regimes. However, due to the finite-size and finite time effects, a higher degree (than the theoretical prediction) operation can help to remove the influence of macroscopic structure on the scaling behavior. To demonstrate this point explicitly, we have drawn $w^2[Q=3](l,t)$ in Fig. 8, of which the transition from the transient regime to the saturated regime is much sharper.

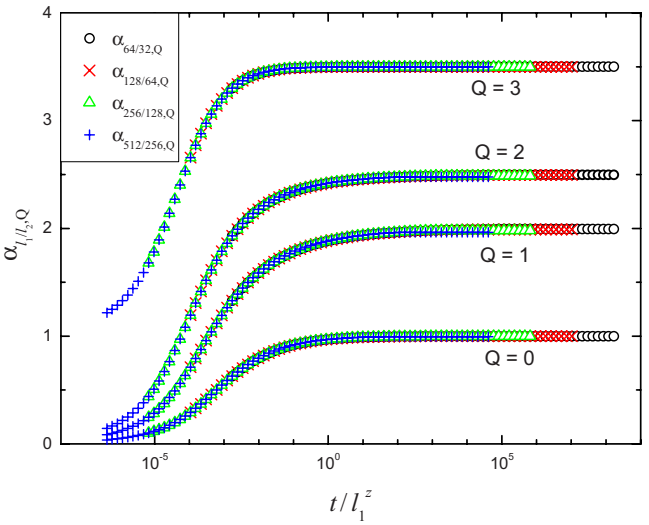

FIG. 9. (Color online) Data collapse of $\alpha_{l_1/l_2,Q}(t)$ vs t/l_1^z in a linear-log plot for the growth processes governed by Eq. (1) with the global roughness exponent $\alpha=2.5$ and the dynamic exponent $z=4$. The data are generated with the parameter $m=2$, the substrate dimension $d=2$, the noise correlation indices $(\rho,\theta)=(0.3,0.3)$, and the lateral linear size of the substrate $L=2^{13}$ sites. For visual clarity, the data for $Q=3$ are shifted upward by one unit.

Now, we will turn to discuss the method of measuring the roughness exponent. The traditional method is to draw the log-log plot of $w^2(l,t)$ vs l and perform the fit of $w^2(l,t) \sim l^{2\alpha_{\rm loc}}$ in the range of $l \ll t^{1/z}$. As pointed out in Ref. [43], this conventional method of measuring the roughness exponent is not reliable if the system consists of long crossover behavior. The authors of Ref. [43] have proposed another method of measurement: Introduce $\alpha_{\rm eff}(l,t) \equiv \frac{\Delta_l[\log w(l,t)]}{\Delta_l(\log l)}$ with Δ_l denoting the difference operator. Draw the plot of $\frac{\Delta_l[\alpha_{\rm eff}(l,t)]}{\Delta_l(\log l)}$ vs $\alpha_{\rm eff}(l,t)$, and the $\alpha_{\rm eff}(l,t)$ corresponding to the minimum of $\frac{\Delta_l[\alpha_{\rm eff}(l,t)]}{\Delta_l(\log l)}$ indicates the value of the local roughness exponent. For normal rough interfaces, the global roughness exponent α is equal to the local roughness exponent $\alpha_{\rm loc}$, and the method proposed in Ref. [43] is indeed more reliable than the traditional method for measuring the roughness exponent. However, for super-rough interfaces, the global roughness exponent α is different from the local roughness exponent $\alpha_{\rm loc}$. A different statistical measure [29], based on the properties of the residual local interfacial width, is capable of measuring both exponents α and $\alpha_{\rm loc}$. Introduce $\alpha_{l_1/l_2,Q}(t) \equiv \log\{w[Q](l_1,t)/w[Q](l_2,t)\}/\log(l_1/l_2)$ and draw the linear-log plot of $\alpha_{l_1/l_2,Q}(t)$ vs t/l_1^z. The saturated value of $\alpha_{l_1/l_2,Q=0}(t)$ gives the value of the local roughness exponent. Subsequently, the $[Q]$-th degree operation (with increasing value of Q) is performed until the saturated value of $\alpha_{l_1/l_2,Q}(t)$ is independent of Q. This value corresponds to the global roughness exponent. For illustration, Fig. 9 shows the data collapse of $\alpha_{l_1/l_2,Q}(t)$ vs t/l_1^z in a linear-log plot for the growth processes governed by Eq. (1) with the global roughness exponent $\alpha=2.5$. In Fig. 9, the data for $Q=3$ are shifted upward by one unit for visual clarity. Theoretically, the saturated value of $\alpha_{l_1/l_2,Q=2}(t)$ is sufficient to give the value of the global roughness exponent. Due to finite-size and finite time effects, the data for $Q=3$ give much sharper transition from the transient regime to saturation. Finally, we note that all these numerical calculations of $w^2(l,t)$ and $w^2[Q](l,t)$ (with arbitrary values of l, t, L, Q, and substrate dimension) are executed according to our proposed algorithm, which will be derived in detail in the next section.

III. NUMERICAL ALGORITHM

Through analytical derivation, the asymptotes of various statistical quantities (such as the correlation function and the interfacial width) can be obtained. However, if one is interested in the full time evolution of these physical quantities, including the crossover behavior, a numerical calculation must be undertaken. In the literature, the most commonly adopted strategy is to perform numerical integration on the original growth equations via the finite difference method, which is the discretization of stochastic partial differential equations on the space-time grid points. This concept of numerical integration is very straightforward and natural. In addition, this method is renowned with its general applicability for study of various growth processes. However, the most frequently faced problem by this way of approach is its huge consumption of CPU time, as pointed out in the past literature. For the substrate dimension $d \geq 2$, the lateral linear size of the system in simulation is usually quite small, due to the concern of computation cost. The situation becomes even severer if the system consists of long crossover behavior. Therefore, it will be valuable if one can devise other numerical algorithms (having the merits of efficiency and precision at the same time) for the specific classes of growth processes. In the following, we aim to develop such an efficient numerical scheme, capable of generating the full time dynamics of interface configurations, the structure factor, the equal-time height difference correlation function, the slope-slope correlation function, the interfacial width, and the residual interfacial width for the growth processes described by Eq. (1) in arbitrary dimensions with arbitrarily large lateral side length and growth time.

A. Efficient numerical scheme for generation of interface configuration

In this subsection, we will propose a numerical algorithm to generate interface configurations $\{h(\mathbf{x},t)\}$ of the growth processes governed by Eq. (1). In numerical studies, the space is discretized. The lattice constant is adopted as the spatial unit. The wave-vector in the $\mathbf{k}$-space is then defined as $\mathbf{k_n}=(2\pi n_1/L,\ldots,2\pi n_d/L)$ with n_i being an integer chosen from $(-L/2+1,-L/2+2,\ldots,L/2)$. By employing Eqs. (7) and (8), we have

$$\overline{\tilde{h}(\mathbf{k_n},t)\tilde{h}(\mathbf{k_{n'}},t)} = \left(\prod_{i=1}^{d} L\delta_{n_i,-n_{i'}}\right)\frac{D_\rho}{\nu k_{\mathbf{n}}^{2m+2\rho}} \times \int_0^t d\tau \tau^{2\theta-1}\left[e^{-\nu k_{\mathbf{n}}^{2m}\tau} - e^{-\nu k_{\mathbf{n}}^{2m}(2t-\tau)}\right] \equiv \left(\prod_{i=1}^{d} L\delta_{n_i,-n_{i'}}\right) H(\mathbf{k_n},t). \quad (58)$$

Because all the noises $\eta(\mathbf{x},t)$'s follow the Gaussian distribution, all their linear combinations [including all the real and imaginary parts of $\tilde{h}(\mathbf{k_n},t)$'s] follow the Gaussian distribution. Since the interface heights $h(\mathbf{x},t)$ must be real numbers, Eq. (58) implies: (1) For the $\mathbf{k_n}$ with all n_i's equal to 0 or $L/2$, $\tilde{h}(\mathbf{k_n},t)$ is real with $[\tilde{h}(\mathbf{k_n},t)]^2=L^dH(\mathbf{k_n},t)$. (2) For the other cases, $\tilde{h}(\mathbf{k_n},t)$ is complex with $\mathrm{Re}[\tilde{h}(\mathbf{k_n},t)]\mathrm{Im}[\tilde{h}(\mathbf{k_n},t)]=0$ and $\{\mathrm{Re}[\tilde{h}(\mathbf{k_n},t)]\}^2=\{\mathrm{Im}[\tilde{h}(\mathbf{k_n},t)]\}^2=L^dH(\mathbf{k_n},t)/2$.

Consequently, the scheme to numerically generate interface configurations of these growth processes in a discrete d-dimensional substrate space, with lateral linear size L and periodic boundary conditions, is given as follows. (a) $\tilde{h}(\mathbf{k_0},t)$ is set to zero, because it is irrelevant to the relative heights. (b) For every $\mathbf{k_n}$ with all its components k_i's equal to 0 or π, $\tilde{h}(\mathbf{k_n},t)$ is a real, random Gaussian variable with zero mean and the variance $L^dH(\mathbf{k_n},t)$. All the random variables in this category are mutually independent and are independent of all the random variables in the next category. (c) In the range of $(0<k_1<\pi,-\pi<k_2\leq\pi,\ldots,-\pi<k_d\leq\pi)\cup(k_1=0$ or $\pi,0<k_2<\pi,-\pi<k_3\leq\pi,\ldots,-\pi<k_d\leq\pi)\cup(k_1=0$ or $\pi,k_2=0$ or $\pi,0<k_3<\pi,-\pi<k_4\leq\pi,\ldots,-\pi<k_d\leq\pi)\cup\cdots\cup(k_1=0$ or $\pi,\ldots,k_{d-1}=0$ or $\pi,0<k_d<\pi)$, all the real parts and imaginary parts of $\tilde{h}(\mathbf{k_n},t)$'s are mutually independent random Gaussian variables with zero mean and the variance $L^dH(\mathbf{k_n},t)/2$. (d) For the rest of $\mathbf{k_n}$'s, $\tilde{h}(\mathbf{k_n},t)$ is obtained through the relation $\tilde{h}(\mathbf{k_n},t)^*$ [the complex conjugate of $\tilde{h}(\mathbf{k_n},t)]=\tilde{h}(-\mathbf{k_n},t)$. Finally, after generating all the $\tilde{h}(\mathbf{k_n},t)$'s, the interface heights $h(\mathbf{x},t)$'s in the real space are obtained through the inverse Fourier transform.

Note that, compared with the numerical scheme for generating $1+1$ dimensional interfaces configurations [23], the above step (c) is rather complicated for high dimensional cases. The construction of step (c) is based on considering the property of periodic boundary conditions [i.e., $\tilde{h}(\mathbf{k_n}+2\pi\hat{\mathbf{e}}_i,t)=\tilde{h}(\mathbf{k_n},t)$ for $i=1,\ldots,d$] and Eq. (58) at the same time. The rigorous execution of step (c) is very important in order to generate the correct amount of independent random variables and, henceforth, the accurate $d+1$ dimensional interfacial configurations.

B. Fast numerical algorithm for generation of the structure factor, the correlation function, and the interfacial width

In this subsection, we will derive in detail the algorithm to generate the structure factor $\overline{\tilde{h}(\mathbf{k_n},t)\tilde{h}(-\mathbf{k_n},t)}$, the equal-time height difference correlation function $G(\mathbf{r},t)$, the slope-slope correlation function $S(\mathbf{r},t)$, the square of local interfacial width $w^2(l,t)$, and the square of residual local interfacial width $w^2[Q](l,t)$ with high speed and precision at the same time.

1. Exact expressions of $G(\mathbf{r},t)$, $S(\mathbf{r},t)$, $w^2(l,t)$, and $w^2[Q](l,t)$ in terms of the structure factor

First, let us recast the expressions of $G(\mathbf{r},t)$, $S(\mathbf{r},t)$, $w^2(l,t)$, and $w^2[Q](l,t)$ in terms of the structure factors $\overline{\tilde{h}(\mathbf{k_n},t)\tilde{h}(-\mathbf{k_n},t)}$. From the definition of $G(\mathbf{r},t)$ and with some calculation, we have

$$G(\mathbf{r},t)=\frac{2}{L^{2d}}\sum_{\mathbf{n}\neq\mathbf{0}}[1-\cos(\mathbf{k_n}\cdot\mathbf{r})]\overline{\tilde{h}(\mathbf{k_n},t)\tilde{h}(-\mathbf{k_n},t)}. \quad (59)$$

Accordingly, from Eqs. (45) and (59), one gets the slope-slope correlation function

$$S(\mathbf{r},t)=\frac{1}{L^{2d}}\sum_{\mathbf{n}\neq\mathbf{0}}[k_{\mathbf{n}}^2\cos(\mathbf{k_n}\cdot\mathbf{r})]\overline{\tilde{h}(\mathbf{k_n},t)\tilde{h}(-\mathbf{k_n},t)}. \quad (60)$$

By employing Eqs. (50) and (59), the expression of the local interfacial width $w(l,t)$ is recast as

$$\begin{aligned}w^2(l,t)&=\frac{1}{L^{2d}}\sum_{\mathbf{n}\neq\mathbf{0}}\left\{\left[\prod_{i=1}^{d}\int_0^l dr_i\frac{2(l-r_i)}{l^2}\right]\times[1-\cos(\mathbf{k_n}\cdot\mathbf{r})]\right\}\overline{\tilde{h}(\mathbf{k_n},t)\tilde{h}(-\mathbf{k_n},t)}\\&=\frac{1}{L^{2d}}\sum_{\mathbf{n}\neq\mathbf{0}}\left\{1-\prod_{i=1}^{d}\frac{2[1-\cos(k_{n_i}l)]}{k_{n_i}^2l^2}\right\}\times\overline{\tilde{h}(\mathbf{k_n},t)\tilde{h}(-\mathbf{k_n},t)}. \quad (61)\end{aligned}$$

Next, by using Eqs. (56) and (59), we can rewrite the $[Q]$-th degree residual local interfacial width as

$$\begin{aligned}w^2[Q](l,t)&=\frac{1}{L^{2d}}\sum_{\mathbf{n}\neq\mathbf{0}}\left\{\sum_{|\mathbf{q}|\leq Q}\left[\prod_{i=1}^{d}\int_0^l dr_i\frac{F_{q_i}(r_i)}{l^2}\right]\times[1-\cos(\mathbf{k_n}\cdot\mathbf{r})]\right\}\overline{\tilde{h}(\mathbf{k_n},t)\tilde{h}(-\mathbf{k_n},t)}\\&=\frac{1}{L^{2d}}\sum_{\mathbf{n}\neq\mathbf{0}}\left\{1-\sum_{|\mathbf{q}|\leq Q}\left[\prod_{i=1}^{d}\frac{\tilde{F}_{q_i}(k_{n_i},l)}{l^2}\right]\right\}\times\overline{\tilde{h}(\mathbf{k_n},t)\tilde{h}(-\mathbf{k_n},t)} \quad (62)\end{aligned}$$

with

$$F_q(r)\equiv 2(2q+1)\int_{-l/2}^{l/2-r}dx P_q\left(\frac{2x}{l}\right)P_q\left(\frac{2x+2r}{l}\right) \quad (63)$$

and

$$\tilde{F}_q(k,l)\equiv\int_0^l dr F_q(r)\cos(kr). \quad (64)$$

For illustration, we explicitly list some of $\tilde{F}_q(k,l)$ as follows:

$$\tilde{F}_0(k,l)=\frac{2}{k^2}(1-\cos kl),$$

$$\tilde{F}_1(k,l)=\frac{6}{k^2}(1+\cos kl)-\frac{24}{k^3l}\sin kl+\frac{24}{k^4l^2}(1-\cos kl),$$

$$\tilde{F}_2(k,l) = \left(\frac{10}{k^2} + \frac{1440}{k^6 l^4}\right)(1 - \cos kl) + \left(\frac{120}{k^3 l} - \frac{1440}{k^5 l^3}\right)\sin kl + \frac{120}{k^4 l^2}(1 + 5\cos kl). \quad (65)$$

Note that the above derived expressions of $G(\mathbf{r},t)$, $S(\mathbf{r},t)$, $w^2(l,t)$, and $w^2[Q](l,t)$ in terms of the structure factors are concise, exact, and *generally applicable to any fluctuating systems*: All these statistical quantities can be expressed as the summation over the structure factors with some specific correlation weights. Hence, the key point of the whole issue is how to obtain the values of the structure factors with high efficiency and precision at the same time.

For the growth processes described in this paper, the structure factor is given in Eq. (58) with

$$H(\mathbf{k}_\mathbf{n},t) = \frac{D_\rho}{\nu k_\mathbf{n}^{2m+2\rho}}\int_0^t d\tau \tau^{2\theta-1}[e^{-\nu k_\mathbf{n}^{2m}\tau} - e^{-\nu k_\mathbf{n}^{2m}(2t-\tau)}] = \frac{D_\rho}{\nu^{1+2\theta}k_\mathbf{n}^{2m+2\rho+4m\theta}}\int_0^{\nu k_\mathbf{n}^{2m}t} d\tau' (\tau')^{2\theta-1}[e^{-\tau'} - e^{-(2\nu k_\mathbf{n}^{2m}t-\tau')}] \equiv \frac{D_\rho}{\nu^{1+2\theta}k_\mathbf{n}^{2m+2\rho+4m\theta}}\mathcal{T}_\theta(\nu k_\mathbf{n}^{2m}t). \quad (66)$$

Since the calculation of $G(\mathbf{r},t)$, $S(\mathbf{r},t)$, $w^2(l,t)$, and $w^2[Q](l,t)$ involves the whole spectrum of the structure factors, the direct numerical integration to obtain the values of $\mathcal{T}_\theta(\nu k_\mathbf{n}^{2m}t)$ for all $\mathbf{k}_\mathbf{n}$'s will take tremendous CPU time. Therefore, the key issue becomes how to quickly and accurately evaluate the values of $\mathcal{T}_\theta(\nu k_\mathbf{n}^{2m}t)$ for all $\mathbf{k}_\mathbf{n}$'s. Once this goal is achieved, all the related statistical quantities can be readily obtained.

2. Efficient method for calculation of $\mathcal{T}_\theta(u)$ and comparison with traditional method of numerical integration

We will first take a rigorous analysis on the properties of the function $\mathcal{T}_\theta(u)$ in order to propose a good numerical scheme. From $\frac{d}{du}\mathcal{T}_\theta(u) = 2e^{-2u}\int_0^u e^\tau \tau^{2\theta-1}d\tau > 0$ for all $u>0$, one observes that the function $\mathcal{T}_\theta(u)$ is a strictly increasing function of u and $\frac{d}{du}\mathcal{T}_\theta(u)$ exponentially decreases to zero as u goes to infinity. If the allowed relative error of $\mathcal{T}_\theta(u)$ is $O(\epsilon)$, one has $\mathcal{T}_\theta(u>u_0) \approx \mathcal{T}_\theta(u\to\infty) = \Gamma(2\theta)$ with the value of u_0 determined by the criterion $\mathcal{T}_\theta(u_0) \geq \Gamma(2\theta)(1-\epsilon)$. For example, the value of $u_0 \approx 18$ is obtained for the noise correlation index $\theta=0.2$ and the allowed relative error of $\mathcal{T}_\theta(u)$ being $\epsilon = 10^{-8}$.

For $u \leq u_0$, we first recast $\mathcal{T}_\theta(u)$ as

$$\mathcal{T}_\theta(u) = u^{2\theta}\int_0^1 d\tau \tau^{2\theta-1}[e^{-u\tau} - e^{-u(2-\tau)}]. \quad (67)$$

Due to the concern about CPU cost, we decide to perform the series expansion on the integrand of Eq. (67), instead of direct numerical integration. However, there exist many options for choosing the expansion (i.e., through $e^{-u(2-\tau)} = e^{-u(2-x)}\sum_{j=0}^\infty \frac{(\tau-x)^j}{j!}u^j$ for any real number x). To ensure the choice of expansion having the merits of computational efficiency and high precision at the same time, we then choose the expansion according to the following criteria: (a) easy to estimate the precision of finite-sum approximation, (b) quick convergence of series and low computation load for calculating the coefficient of each term in the series. After a few trials, we choose the following series expansion for $\mathcal{T}_\theta(u)$,

$$\mathcal{T}_\theta(u) = u^{2\theta}\sum_{j=0}^\infty \frac{u^j}{j!}\int_0^1 d\tau \tau^{2\theta-1}\tau^j[(-1)^j - e^{-2u}] = u^{2\theta}\sum_{j=0}^\infty \frac{u^j}{j!}\frac{(-1)^j - e^{-2u}}{j+2\theta} \equiv \lim_{N\to\infty}\sum_{j=0}^N A_j(u) \equiv \lim_{N\to\infty} S_N(u). \quad (68)$$

This series converges for all $0 \leq u < \infty$. $A_j(u)$ is obviously a sequence of alternating sign for $u>0$ and $0<\theta<1/2$. In addition, with $0<\theta<1/2$, one gets

$$\left|\frac{A_{2j+1}(u)}{A_{2j}(u)}\right| = \frac{(2j+2\theta)u}{(2j+1)(2j+1+2\theta)\tanh u} \leq \begin{cases} \frac{1}{(2j+1)\tanh 1}\left(\simeq \frac{1.313}{2j+1}\right), & \text{for } 0<u\leq 1, \\ \frac{u}{(2j+1)\tanh 1}\left(\simeq \frac{1.313u}{2j+1}\right), & \text{for } u>1; \end{cases} \quad (69)$$

and

$$\left|\frac{A_{2j}(u)}{A_{2j-1}(u)}\right| = \frac{(2j-1+2\theta)u\tanh u}{2j(2j+2\theta)} \leq \begin{cases} \frac{u\tanh 1}{2j}\left(\simeq \frac{0.7616u}{2j}\right), & \text{for } 0<u\leq 1, \\ \frac{u}{2j}, & \text{for } u>1. \end{cases} \quad (70)$$

Consequently, the value of $|A_j(u)|$ decreases as j increases for $u>0$ and $j>1.313\max(1,u)$. Thus, we derive that the value of $|A_N/S_N|$ can be taken as an upper bound to evaluate the relative discrepancy between the partial series and the whole series for $N>1.313\max(1,u)$.

Note that this series expansion of $\mathcal{T}_\theta(u)$ is a very fast convergent series for $u \leq u_0$. For example, to keep the relative error of $\mathcal{T}_\theta(u)$ less than 10^{-8}, a partial sum of 2 terms is sufficient for $u \lesssim 2.5\times 10^{-4}$, a partial sum of $3\sim 10$ terms is sufficient for $2.5\times 10^{-4} \lesssim u \lesssim 1$, and a partial sum of $11\sim 38$ terms is sufficient for $1 \lesssim u \lesssim 10$. Even if u is as large as $18 \approx u_0$, a partial sum of 61 terms is sufficient to keep the relative error less than 10^{-8}. In addition, the evaluation of the partial sum can be further simplified by executing the following three steps: (a) Calculate the exponential e^{-2u} (which can be reused for the whole procedure), set $\tilde{S}_0 = (1-e^{-2u})/(2\theta)$, and set $w_0=1$. (b) Execute the following loop $\{w_{j+1} = \frac{w_j\cdot u}{j+1}, \tilde{S}_{j+1} = \tilde{S}_j + w_{j+1}\cdot\frac{(-1)^{j+1}-e^{-2u}}{j+1+2\theta}\}$. (c) Once the precision goal is reached, terminate the loop and multiply the factor $u^{2\theta}$ to

the final estimate $\tilde{S}_N$. In the steps mentioned above, only simple summation, multiplication, and division are involved.

Remarkably, in our proposed scheme, no numerical integration is needed at all. To demonstrate the excellency of our method for calculation of $\mathcal{T}_\theta(u)$ over the traditional method of numerical integration adopted in the commercial softwares such as MATHEMATICA [45,46], we explicitly compare these two methods in detail in the following. The basic strategies of numerical integration adopted in MATHEMATICA are summarized as follows. In MATHEMATICA, the command for numerical integration is "NIntegrate," whose default rule is the Gauss-Kronrod integration method with the global adaptive strategy. The Kronrod result and its difference from the Gauss result are used as the integral estimate and the error estimate, respectively. The spirit of the global adaptive strategy is aimed to improve the integral estimate through recursive bisection. More specifically, it first evaluates the integrand at 11 quadrature points (5 Gauss quadrature points and 6 Kronrod quadrature points) for a prescribed integration interval (after the scale transformation into the interval $[-1,1]$); if the precision goal is not reached, it bisects the integration interval into two halves and reconducts the calculation of the integrand at 22 new quadrature points (11 in each half after the scale transformation of the subinterval into the interval $[-1,1]$). This procedure is repeated until the precision goal is attained. If the integrand contains singularities at the end points of the integration interval, "NIntegrate" of MATHEMATICA employs the Iri-Moriguti-Takasawa (IMT) variable transformation on the integrand to deal with the singularity problem [45,46]. In addition, the default value (equal to 4) of "Singularity Depth" in Mathematica specifies how many levels of subdivision it should perform before adopting the IMT transformation. Namely, if the integrand consists of a singularity at one of the end points of the integration interval, "NIntegrate" of Mathematica will execute the evaluation of the IMT-transformed integrand at 11 quadrature points in the subinterval, one-sixteenth of the original integration interval, and the evaluation of the original integrand at 88 quadrature points for the most optimistic case.

Note that the integrand given in Eq. (67), $\tau^{2\theta-1}[e^{-u\tau}-e^{-u(2-\tau)}]$, consists of a singularity at $\tau=0$ (the lower end point of the integration interval). By employing the IMT transformation rule given in MATHEMATICA [45], the IMT-transformed integrand is derived as $(16^\theta v)^{-2}e^{2\theta(1-1/v)}[e^{-ue^{(1-1/v)}/16}-e^{-u(2-e^{(1-1/v)}/16)}]$, where v is the transformed variable to be integrated from 0 to 1. One can clearly see that the IMT-transformed integrand is much more complicated and incurs additional computational load. In words, "NIntegrate" of Mathematica needs to evaluate the integrand at least for 99 quadrature points to get the estimated value of $\mathcal{T}_\theta(u)$ for a given u. The evaluation of $\tau^{2\theta-1}[e^{-u\tau}-e^{-u(2-\tau)}]$ at each quadrature point involves three exponentiations, since the value of τ is different at different quadrature points. Moreover, the evaluation of the IMT-transformed integrand requires even more computational load. By contrast, in our proposed algorithm, relatively few terms of the partial sum for $\mathcal{T}_\theta(u)$ are sufficient to fulfill the precision goal. Furthermore, in our algorithm, we only need to calculate the exponentiations (e^{-2u} and $u^{2\theta}$) for once at a given u and the calculation of each term in the partial sum of $\mathcal{T}_\theta(u)$ only involves simple summation, multiplication, and division. Therefore, our proposed scheme is definitely much more efficient (without the sacrifice of precision) than the traditional method of numerical integration adopted in the commercial softwares such as MATHEMATICA.

3. Quick way for evaluation of the full time evolution of $G(\mathbf{r},t)$, $S(\mathbf{r},t)$, $w^2(l,t)$, and $w^2[Q](l,t)$

With all the obtained results in this subsection, an algorithm to rapidly obtain the full time evolution of $G(\mathbf{r},t)$, $S(\mathbf{r},t)$, $w^2(l,t)$, and $w^2[Q](l,t)$ can be executed according to the following steps: (a) Since all these statistical quantities can be viewed as weighted sums of the structure factors $\{H(\mathbf{k_n},t)\}$ with certain correlation weights (which are functions of $\{k_{n_i}r_i\}$ or $\{k_{n_i}l\}$) over the $\mathbf{k}$-space, one can first build up a table for the correlation weights over the $\mathbf{k}$-space. (b) By recalling $\mathbf{k_n}=\frac{2\pi}{L}(n_1,\ldots,n_d)$ with $n_i=-L/2+1,\ldots,L/2$, one gets $\nu k_{2^j\mathbf{n}}^{2m}t=\nu k_{\mathbf{n}}^{2m}(2^{2mj}t)$. In addition, with the property $\mathcal{T}_\theta(u>u_0)\approx\Gamma(2\theta)$, it implies that we only need to evaluate the values of $\mathcal{T}_\theta(\nu k_{\mathbf{n}}^{2m}t_0)$ for all $\mathbf{k_n}$'s and, then, all the values of $\mathcal{T}_\theta(\nu k_{\mathbf{n}}^{2m}t_j)$ with $t_j=2^{2mj}t_0$ are readily obtained. (c) Moreover, the evaluation of $\mathcal{T}_\theta(\nu k_{\mathbf{n}}^{2m}t_0)$ for all $\mathbf{k_n}$'s can be further simplified. From the symmetry consideration, we actually only need to evaluate the values of $\mathcal{T}_\theta(\nu k_{\mathbf{n}}^{2m}t_0)$ with $n_1\geq n_2\geq\cdots\geq n_d\geq 0$ and $\nu k_{\mathbf{n}}^{2m}t_0\leq u_0$. Consequently, the number of irreducible points of $\mathcal{T}_\theta(u)$ need to be explicitly evaluated are actually just $[d!\Gamma(\frac{d}{2}+1)]^{-1}(\frac{L}{4\sqrt{\pi}})^d(\frac{u_0}{\nu t_0})^{d/(2m)}$. One can then build up a table for these $\mathcal{T}_\theta(u)$'s. (d) By combining the tables in (a) and (c) with appropriate scale transformation, the full time evolution of $G(\mathbf{r},t)$, $S(\mathbf{r},t)$, $w^2(l,t)$, and $w^2[Q](l,t)$ are quickly obtained.

For example, with ($\nu=1$, $m=2$, $d=2$, $\theta=0.3$, $L=2^{13}$, and $t_0=2^{15}$) as the parameters given in Figs. 2, 8, and 9, the number of irreducible points of $\mathcal{T}_\theta(u)$ in the three subregions of u ($0\lesssim u\lesssim 2.5\cdot 10^{-4}$, $2.5\cdot 10^{-4}\lesssim u\lesssim 1$, and $1\lesssim u\lesssim u_0\approx 18$) are 60, 3600, and 12000, respectively. Remarkably, with such few irreducible points of $\mathcal{T}_\theta(u)$, we can generate the whole data set of Figs. 2, 8, and 9 with $t=2^{15}\sim 2^{50}$ time steps. In words, although one can analytically derive the asymptotes for linear growth processes, numerical simulation with large system size and growth time is still necessary if the system consists of long initial transients before entering scaling regimes, long crossover between two scaling regimes, or large correction to scaling due to finite-size effects. Note that the CPU time for simulation is approximately proportional to L^d. Hence, an efficient numerical scheme with high precision is very valuable, especially for high spatial dimensions. To demonstrate the effectiveness and accuracy of our algorithm through explicit examples, all the data in the figures related to Eq. (1) are generated according to the above algorithm. They only consume very modest computation time by a desktop PC, even for a two-dimensional substrate space with such large lateral linear size $L=2^{15}$ sites and growth time $t=2^{60}$ steps.

Many physical processes in various fields [47] can be described by linear stochastic partial differential equations with

the mathematical forms similar to Eq. (1); for instance, the evolution of the temperature field of a flat plate heat-treated by a laser beam whose intensity is overall uniform with some correlated random fluctuations, or the evolution of phase separation of a binary mixture through the mechanism of heterogeneous nucleation induced by the presence of annealed dust particles. The generalization of our numerical scheme to other linear stochastic partial differential equations is straightforward. Furthermore, note that some classes of nonlinear stochastic partial differential equations can be transformed to linear stochastic partial differential equations through appropriate transformations. For instance, consider the following class of nonlinear stochastic partial differential equations, $f(v)\frac{\partial v(\mathbf{x},t)}{\partial t}=(-1)^{m+1}\nu\nabla^{2m-2}\vec{\nabla}\cdot[f(v)\vec{\nabla}v(\mathbf{x},t)]+\eta(\mathbf{x},t)$ with the function $f(\cdot)>0$. The transformation $h=\int_0^v f(v')dv'$ $[\equiv g(v)]$ ensures the quantity h having a one-to-one correspondence with the quantity v. By simply substituting $h=g(v)$ into Eq. (1), one readily obtains the above nonlinear stochastic partial differential equation and *the noise form is unaltered through the transformation*. Consequently, by employing the relation $v=g^{-1}(h)$, our numerical scheme can also be applied to some classes of nonlinear equations.

IV. CONCLUSION

In conclusion, we take an extensive analytical and numerical study on the growth processes in $d+1$ dimensions, governed by Eq. (1) with spatiotemporally correlated noises. This class of growth processes displays a family of continuously changing universality classes. Specifically, the global roughness exponent is a strictly increasing function of the noise correlation indices (ρ,θ) for the whole range. The aim of Eq. (1) is to give a generic phenomenological continuum description of both stable surface growth and unstable surface growth, without referring to atomistic details. Various experiments in different fields, ranging from materials science to cell biology, can be well described by Eq. (1). Although the experimental realizations for Eq. (1) with $m>3$ have not yet been established, this study is still very valuable. Since Eq. (1) is exactly solvable, it can help us to obtain a more complete picture about the interplay of the following effects: local interfacial height correlation, the substrate dimensionality, and the noise correlation. Moreover, Eq. (1) also offers a perfect test ground for our proposed statistical methods (explained in Sec. II and III), due to its exact solvability.

First, we give a rigorous and extensive analytical derivation of the asymptotes of the equal-time height difference correlation function $G(\mathbf{r},t)$, the slope-slope correlation function $S(\mathbf{r},t)$, and the local interfacial width $w(l,t)$ in successive time regimes for arbitrary substrate dimensionality. Based on the above analysis, we give a plausible theoretical explanation and a unified picture about the various experimental observations of kinetically and thermodynamically unstable surface growth, ranging from electrochemical deposition to molecular-beam epitaxy for many different materials: (a) The characteristic lateral linear scale of hills (or valleys) grows with time according to $(\nu t)^{1/(2m)}$, which will develop faster in time with the increasing substrate temperature. (b) The average local inclination of hills increases in time with the leading power-law exponents $\{\frac{1}{2}+\theta-\frac{i+d/2-\rho}{2m};i=1,2,\ldots,[\alpha]\}$. We give a detailed argument why this quantity will definitely develop faster in time by enhancing the deposition flux but it may grow either faster or slower in time if the substrate temperature increases. (c) The dimensionality has relative minor influence on the lateral development of hills and valleys, but it has strong influence on the temporal development of local inclination of hills (or valleys). Furthermore, recall that the correction terms to scaling in equilibrium critical phenomena may correspond to a logarithmic correction, to a cusplike correction, or even to a jump discontinuity. Here, we rigorously show that the dynamic scaling behaviors of the growth processes governed by Eq. (1) uniquely display logarithmic corrections if the exponent α is an integer. Moreover, in the process of derivation, we even derive a new mathematical formula (given in the Appendix).

In the numerical or experimental study of interface growth, it is essential that the statistical methods of determining the values of the scaling exponents and various important physical quantities indeed give reliable estimates. Inspired by the works of Refs. [24–26], we rigorously study the properties of the slope-slope correlation function $S(\mathbf{r},t)$. First, we observe that the first zero of the slope-slope correlation function gives a quantitatively precise and objective measurement of the correlation length. Through various numerical examples, we conclude that the method of determining the dynamic exponent based on $r_0(t)$ is superior to other traditional methods in the literature. Its most distinct feature is that the relation $r_0(t)\propto t^{1/z}$ extends the whole temporal range (not just the asymptotic behavior) before the correlation length reaching the lateral linear size of the system. Furthermore, due to the excellency of determining the dynamic exponent z based on $r_0(t)$, our numerical results resolve the long debate about the universality class of $2+1$ dimensional DT model in the literature. We clearly observe that the dynamic exponent z indeed changes from 4 to 10/3, fully confirming the prediction of the VLDS equation. Remarkably, we also observe that the functional shape of $S(r,t)$, in the region of $r<r_0(t)$, has a signature difference between stable surface growth and unstable surface growth. Note that this qualitative difference is independent of the substrate dimensionality or other details of growth conditions. The only relevant factor is the value of the exponent α being less or greater than one. By employing this qualitative distinct difference in functional shape of $S(\mathbf{r},t)$, one can easily classify the experimental growth systems into the categories of stable surface growth or unstable surface growth. This method is especially useful for the classification of the experimental growth systems (with the exponent α close to 1) into the correct categories.

For the growth processes with the exponent $\alpha>1$, the macroscopic hills and/or valleys gradually develop and merge as growth time increases. The formation of the macroscopic structure in the interfacial morphology is totally attributed to local interfacial orientational instability. We systematically express the macroscopic structure of the interface configuration in terms of Legendre polynomials order by order. In addition, we also give the explicit relations among the

correlation function, the local interfacial width, and the $[Q]$-th degree residual local interfacial width. The derived relations are exact and generally applicable for any fluctuating systems in arbitrary substrate dimensions. The statistical method, based on the scaling of the $[Q]$-th degree residual local interfacial width, is capable of measuring both the global roughness exponent α and the local roughness exponent α_{loc}. The scheme of operation is very simple: Define $\alpha_{l_1/l_2,Q}(t)=\log[w(Q)(l_1,t)/w(Q)(l_2,t)]/\log(l_1/l_2)$ and draw the linear-log plot of $\alpha_{l_1/l_2,Q}(t)$ vs t/l_1^z. The saturated value of $\alpha_{l_1/l_2,Q=0}(t)$ gives the estimate of the local roughness exponent. Subsequently, the $[Q]$-th degree operation is performed until the saturated value of $\alpha_{l_1/l_2,Q}(t)$ does not alter with Q, which gives the estimate of the global roughness exponent. Through numerical examples, we explicitly demonstrate the excellency of our proposed method. Moreover, we also rigorously derive the exact and explicit expressions of $G(\mathbf{r},t)$, $S(\mathbf{r},t)$, $w^2(l,t)$, and $w^2[Q](l,t)$ in terms of the structure factors. Note that the derived expressions are also generally applicable to any fluctuating systems in arbitrary dimensions.

Another important issue we focus on in this paper is related to the construction of efficient numerical algorithm. The numerical calculation is aimed to obtain the full time evolution of interface dynamics including the early, intermediate, and late-time behaviors. The direct numerical integration of interfacial growth equations via the finite difference method is widely adopted in the literature, due to its simplicity and general applicability. Although the concept of direct numerical integration is quite straightforward, its execution usually takes tremendous CPU time to obtain the whole range of interface dynamics, for the growth processes having large value of dynamic exponent z. Therefore, we propose a very efficient algorithm with high precision (capable of calculating the full time evolution of interface configurations, the structure factor, the equal-time height difference correlation function, the slope-slope correlation function, the local interfacial width, and the $[Q]$-th degree residual local interfacial width) for the class of growth processes discussed in this paper. We then explicitly show that our algorithm is indeed much more efficient than the traditional method of numerical integration adopted in commercial softwares. In addition, our numerical scheme is very systematical and can be easily generalized for other linear processes and some special nonlinear processes. Thus, direct numerical integration can be avoided. However, such an efficient algorithm for general nonlinear growth processes is not yet found. It remains a big challenge for the further work in the field of kinetic interfacial roughening.

ACKNOWLEDGMENTS

The works of N.-N. Pang and W.-J. Tzeng are supported in part by the National Science Council of the Republic of China under Grants No. NSC-97-2112-M002-016-MY3 and No. NSC-97-2112-M032-002-MY3, respectively, and the National Center of Theoretical Sciences in Taipei.

APPENDIX

In this appendix, we will rigorously show that, for α and d being natural numbers,

$$\int_x^\infty x^{-2\alpha-d/2}J_{d/2-1}(x)dx=\sum_{n=0,n\neq\alpha}^{\infty}\frac{(-1)^{n+1}x^{2(n-\alpha)}}{2^{2n+d/2}(n-\alpha)n!\Gamma(n+d/2)}+\frac{(-1)^{\alpha}}{2^{2\alpha+d/2-1}\Gamma(\alpha+1)\Gamma(\alpha+d/2)}(\Omega-\ln x) \tag{A1}$$

with

$$\Omega=\begin{cases}-\gamma+\left(\sum_{n=1}^{\alpha}\frac{1}{2n}\right)+\left(\sum_{n=0}^{\alpha+d/2-3/2}\frac{1}{2n+1}\right), & \text{for } d=1,3,5,\ldots,\\ -\gamma+\ln 2+\left(\sum_{n=1}^{\alpha}\frac{1}{2n}\right)+\left(\sum_{n=1}^{\alpha+d/2-1}\frac{1}{2n}\right), & \text{for } d=2,4,6,\ldots,\end{cases} \tag{A2}$$

and γ being the Euler constant ($\approx$0.577 215 664 9).

(i) First, by employing the relation $\frac{d}{dx}[x^{-\mu}J_\mu(x)]=-x^{-\mu}J_{\mu+1}(x)$ repeatedly, we get

$$\int_x^\infty x^{-2\alpha-d/2}J_{d/2-1}(x)dx=\sum_{n=0}^{\alpha-1}\frac{(-1)^n\Gamma(\alpha-n)}{2^{n+1}\Gamma(\alpha+1)}x^{-2\alpha-d/2+n+1}J_{d/2-1+n}(x)+\frac{(-1/2)^{\alpha}}{\Gamma(\alpha+1)}\int_x^\infty x^{-\alpha-d/2}J_{d/2+\alpha-1}(x)dx\equiv A+B. \tag{A3}$$

Subsequently, by employing the power series expansion of $J_\mu(x)$, the term A can be recast as

$$A = \sum_{j=0}^{\infty} \sum_{n=0}^{\alpha-1} \frac{(-1)^{j+n}\Gamma(\alpha-n)}{2^{2j+2n+d/2}\Gamma(\alpha+1)\Gamma(j+1)\Gamma(j+d/2+n)} x^{2n+2j-2\alpha}$$
$$= \frac{(-1)^{\alpha}}{2^{2\alpha+d/2}\Gamma(\alpha+1)\Gamma(\alpha+d/2)}\left(\sum_{n=1}^{\alpha}\frac{1}{n}\right) + \frac{1}{\Gamma(\alpha+1)}\sum_{n=1}^{\infty}\frac{(-1)^{n+\alpha}x^{2n}}{2^{2n+2\alpha+d/2}n\Gamma(n+1)\Gamma(n+\alpha+d/2)}$$
$$-\left(\sum_{n=-\alpha}^{-1}+\sum_{n=1}^{\infty}\right)\frac{(-1)^{n+\alpha}x^{2n}}{2^{2n+2\alpha+d/2}n\Gamma(n+\alpha+1)\Gamma(n+\alpha+d/2)}. \tag{A4}$$

(ii) Next, by applying the relation $\frac{d}{dx}[x^{\mu}J_{\mu}(x)]=x^{\mu}J_{\mu-1}(x)$ repeatedly, the term B is rewritten as

$$B = \frac{(-1)^{\alpha}}{\Gamma(\alpha+1)}\sum_{n=1}^{\alpha+[(d-1)/2]}\frac{\Gamma(\alpha+d/2-n)}{2^{n+\alpha}\Gamma(\alpha+d/2)}x^{-\alpha-d/2+n}J_{d/2+\alpha-n}(x) + \frac{(-1)^{\alpha}\Gamma\left(\frac{d}{2}-\left[\frac{d-1}{2}\right]\right)}{2^{2\alpha+[(d-1)/2]}\Gamma(\alpha+1)\Gamma(\alpha+d/2)}\int_x^{\infty} x^{-d/2+[(d-1)/2]}J_{(d/2)-1-[(d-1)/2]}(x)dx$$
$$\equiv C + D \tag{A5}$$

with $[\cdot]$ denoting the integer part. For d being an odd positive integer, we have

$$D_{\text{odd}} = \frac{(-1)^{\alpha}\Gamma(1/2)}{2^{2\alpha+d/2-1/2}\Gamma(\alpha+1)\Gamma(\alpha+d/2)}\int_x^{\infty} x^{-1/2}J_{-1/2}(x)dx = \frac{(-1)^{\alpha+1}}{2^{2\alpha+d/2-1}\Gamma(\alpha+1)\Gamma(\alpha+d/2)}\left[\gamma+\ln x+\sum_{n=1}^{\infty}\frac{(-1)^n}{2n(2n)!}x^{2n}\right]; \tag{A6}$$

for d being an even positive integer, we get

$$D_{\text{even}} = \frac{(-1)^{\alpha}}{2^{2\alpha+d/2-1}\Gamma(\alpha+1)\Gamma(\alpha+d/2)}\int_x^{\infty} x^{-1}J_0(x)dx = \frac{(-1)^{\alpha+1}}{2^{2\alpha+d/2-1}\Gamma(\alpha+1)\Gamma(\alpha+d/2)}\left[\gamma+\ln\frac{x}{2}+\sum_{n=1}^{\infty}\frac{(-1)^n}{2n(n!)^2}\left(\frac{x}{2}\right)^{2n}\right], \tag{A7}$$

with γ being the Euler constant.

(iii) Subsequently, by applying the relation $\sum_{n'=0}^{n}\frac{\Gamma(n'+a)}{\Gamma(n'+b)}=\frac{1}{a-b+1}\left[\frac{\Gamma(n+a+1)}{\Gamma(n+b)}-\frac{\Gamma(a)}{\Gamma(b-1)}\right]$ and the power series expansion of $J_{\mu}(x)$, the term C can be recast as

$$C_{\text{odd}} = \frac{(-1)^{\alpha}}{2^{2\alpha+d/2}\Gamma(\alpha+1)\Gamma\left(\alpha+\frac{d}{2}\right)}\left\{\left(\sum_{n=0}^{\alpha+d/2-3/2}\frac{1}{\frac{1}{2}+n}\right)-\sum_{n=1}^{\infty}\frac{(-1)^n x^{2n}}{n2^{2n}n!}\left[\frac{\Gamma\left(\frac{d}{2}+\alpha\right)}{\Gamma\left(n+\frac{d}{2}+\alpha\right)}-\frac{\Gamma\left(\frac{1}{2}\right)}{\Gamma\left(n+\frac{1}{2}\right)}\right]\right\} \tag{A8}$$

for d being an odd positive integer, and

$$C_{\text{even}} = \frac{(-1)^{\alpha}}{2^{2\alpha+d/2}\Gamma(\alpha+1)\Gamma\left(\alpha+\frac{d}{2}\right)}\left\{\left(\sum_{n=1}^{\alpha+\frac{d}{2}-1}\frac{1}{n}\right)-\sum_{n=1}^{\infty}\frac{(-1)^n x^{2n}}{n2^{2n}n!}\left[\frac{\Gamma\left(\frac{d}{2}+\alpha\right)}{\Gamma\left(n+\frac{d}{2}+\alpha\right)}-\frac{1}{n!}\right]\right\} \tag{A9}$$

for d being an even positive integer.

(iv) We finally obtain, with α being a positive integer,

$$\int_x^{\infty} x^{-2\alpha-d/2}J_{d/2-1}(x)dx = A + C_{\text{odd}} + D_{\text{odd}} = \left(\sum_{n=-\alpha}^{-1}+\sum_{n=1}^{\infty}\right)\frac{(-1)^{n+\alpha+1}x^{2n}}{2^{2n+2\alpha+d/2}n(n+\alpha)!\Gamma(n+\alpha+d/2)} - \frac{(-1)^{\alpha}}{2^{2\alpha+d/2}\Gamma(\alpha+1)\Gamma(\alpha+d/2)}$$
$$\times\left[2\gamma+2\ln x-\left(\sum_{n=1}^{\alpha}\frac{1}{n}\right)-\left(\sum_{n=0}^{\alpha+d/2-3/2}\frac{1}{n+1/2}\right)\right] \tag{A10}$$

for d being an odd positive integer, and

$$\int_x^\infty x^{-2\alpha-d/2} J_{d/2-1}(x)dx = A + C_{\text{even}} + D_{\text{even}} = \left(\sum_{n=-\alpha}^{-1} + \sum_{n=1}^{\infty}\right) \frac{(-1)^{n+\alpha+1} x^{2n}}{2^{2n+2\alpha+d/2} n(n+\alpha)!\Gamma(n+\alpha+d/2)} - \frac{(-1)^{\alpha}}{2^{2\alpha+d/2}\Gamma(\alpha+1)\Gamma(\alpha+d/2)}$$
$$\times \left[2\gamma + 2\ln\frac{x}{2} - \left(\sum_{n=1}^{\alpha} \frac{1}{n}\right) - \left(\sum_{n=1}^{\alpha+d/2-1} \frac{1}{n}\right) \right] \tag{A11}$$

for d being an even positive integer. With the rearrangement of the summation indices in the above two equations, we consequently derive the relations, Eqs. (A1) and (A2).

[1] T. Dobrowolski, Eur. Phys. J. B **29**, 269 (2002).
[2] M. Cattani and M. C. Salvadori, Thin Solid Films **376**, 264 (2000).
[3] S. Alonso, I. Sendiña-Nadal, V. Pérez-Muñuzuri, J. M. Sancho, and F. Sagués, Phys. Rev. Lett. **87**, 078302 (2001).
[4] H. Sompolinsky, H. Yoon, K. Kang, and M. Shamir, Phys. Rev. E **64**, 051904 (2001).
[5] B. Röseler and C. A. Schiller, Mater. Corros. **52**, 413 (2001).
[6] H.-N. Yang, Y.-P. Zhao, G.-C. Wang, and T.-M. Lu, Phys. Rev. Lett. **76**, 3774 (1996).
[7] J.-H. Jeffries, J. K. Zuo, and M. M. Craig, Phys. Rev. Lett. **76**, 4931 (1996).
[8] S. Bahar, J. W. Kantelhardt, A. Neiman, H. H. A. Rego, D. F. Russell, L. Wilkens, A. Bunde, and F. Moss, EPL **56**, 454 (2001).
[9] A. Bunde, S. Havlin, J. W. Kantelhardt, T. Penzel, J.-H. Peter, and K. Voigt, Phys. Rev. Lett. **85**, 3736 (2000).
[10] M. Saitou, Phys. Rev. B **66**, 073416 (2002).
[11] T. Boyer, S. Levitus, H. Garcia, R. A. Locarnini, C. Stephens, and J. Antonov, Int. J. Climatol. **25**, 931 (2005).
[12] J. A. Stroscio, D. T. Pierce, M. D. Stiles, A. Zangwill, and L. M. Sander, Phys. Rev. Lett. **75**, 4246 (1995).
[13] J. E. Van Nostrand, S. Jay Chey, M.-A. Hasan, D. G. Cahill, and J. E. Greene, Phys. Rev. Lett. **74**, 1127 (1995).
[14] M. D. Johnson, C. Orme, A. W. Hunt, D. Graff, J. Sudijono, L. M. Sander, and B. G. Orr, Phys. Rev. Lett. **72**, 116 (1994).
[15] H.-J. Ernst, F. Fabre, R. Folkerts, and J. Lapujoulade, Phys. Rev. Lett. **72**, 112 (1994).
[16] K. Thürmer, R. Koch, M. Weber, and K. H. Rieder, Phys. Rev. Lett. **75**, 1767 (1995).
[17] S. F. Edwards and D. R. Wilkinson, Proc. R. Soc. London, Ser. A **381**, 17 (1982).
[18] W. W. Mullins, J. Appl. Phys. **28**, 333 (1957).
[19] D. E. Wolf and J. Villain, EPL **13**, 389 (1990).
[20] A. Brú, J. M. Pastor, I. Fernaud, I. Brú, S. Melle, and C. Berenguer, Phys. Rev. Lett. **81**, 4008 (1998).
[21] J. Stewart and N. Goldenfeld, Phys. Rev. A **46**, 6505 (1992).
[22] F. Liu and H. Metiu, Phys. Rev. B **48**, 5808 (1993).
[23] N.-N. Pang and W.-J. Tzeng, Phys. Rev. E **70**, 011105 (2004).
[24] M. Siegert and M. Rao, Phys. Rev. Lett. **70**, 1956 (1993).
[25] M. Siegert and M. Plischke, Phys. Rev. Lett. **73**, 1517 (1994).
[26] G. Palasantzas, Solid State Commun. **100**, 699 (1996).
[27] T. Halpin-Healy and Y.-C. Zhang, Phys. Rep. **254**, 215 (1995).
[28] S. Das Sarma, C. J. Lanczycki, R. Kotlyar, and S. V. Ghaisas, Phys. Rev. E **53**, 359 (1996).
[29] N.-N. Pang and W.-J. Tzeng, Phys. Rev. E **70**, 036115 (2004).
[30] E. Medina, T. Hwa, M. Kardar, and Y.-C. Zhang, Phys. Rev. A **39**, 3053 (1989).
[31] H. K. Janssen, U. C. Täuber, and E. Frey, Eur. Phys. J. B **9**, 491 (1999).
[32] J. Spanier and K. B. Oldham, *An Atlas of Functions* (Hemisphere, Washington, 1987); A. P. Prudnikov, Y. A. Brychkov, and O. I. Marichev, *Integrals and Series* (Gordon and Breach, New York, 1986); I. S. Gradshteyn and I. M. Ryzhik, *Table of Integrals, Series, and Products* (Academic, San Diego, 2007).
[33] H. E. Stanley, *Introduction to Phase Transitions and Critical Phenomena* (Oxford, New York, 1971).
[34] H. Leschhorn and L.-H. Tang, Phys. Rev. Lett. **70**, 2973 (1993).
[35] J. M. López, M. Castro, and R. Gallego, Phys. Rev. Lett. **94**, 166103 (2005).
[36] J. M. López, M. A. Rodríguez, and R. Cuerno, Physica A **246**, 329 (1997).
[37] S. Das Sarma and P. I. Tamborenea, Phys. Rev. Lett. **66**, 325 (1991).
[38] J. Krug, Phys. Rev. Lett. **72**, 2907 (1994).
[39] M. Předota and M. Kotrla, Phys. Rev. E **54**, 3933 (1996).
[40] Z.-F. Huang and B.-L. Gu, Phys. Rev. E **54**, 5935 (1996).
[41] J. Villain, J. Phys. I **1**, 19 (1991); Z.-W. Lai and S. Das Sarma, Phys. Rev. Lett. **66**, 2348 (1991).
[42] S. Das Sarma, P. P. Chatraphorn, and Z. Toroczkai, Phys. Rev. E **65**, 036144 (2002).
[43] A. Chame and F. D. A. Aarão Reis, Surf. Sci. **553**, 145 (2004).
[44] N.-N. Pang, W.-J. Tzeng, and H.-C. Kao, Phys. Rev. E **78**, 011112 (2008).
[45] The website is http://reference.wolfram.com/mathematica/tutorial/NIntegrateIntegrationStrategies.html
[46] A. R. Krommer and C. W. Ueberhuber, *Numerical Integration on Advanced Computer Systems* (Springer-Verlag, New York, 1994); R. L. Johnston, *Numerical Methods: A Software Approach* (Wiley, New York, 1982); P. J. Davis and P. Rabinowitz, *Methods of Numerical Integration* (Academic Press, Orlando, 1984).
[47] R. A. L. Jones, *Soft Condensed Matter* (Oxford University Press, Oxford, 2002); S. Kou, *Transport Phenomena and Materials Processing* (Wiley, New York, 1996).